# Data-model discord reveals challenges in reconstructing terrestrial warming of the Pliocene

Ulrich Salzmann[1*], Aisling M. Dolan[2], Alan M. Haywood[2], Wing-Le Chan[3], Daniel J. Hill[4], Jochen Voss[5], Ayako Abe-Ouchi[3,6], Bette Otto-Bliesner[7], Fran Bragg[8], Mark A. Chandler[9], Camille Contoux[10,11], Harry J. Dowsett[12], Anne Jost[11], Youichi Kamae[13], Gerrit Lohmann[14], Daniel J. Lunt[8], Steven J. Pickering[2], Matthew J. Pound[1], Gilles Ramstein[10], Nan A. Rosenbloom[7], Linda Sohl[9], Christian Stepanek[14], Hiroaki Ueda[13], Zhongshi Zhang[15,16]

[1] Department of Geography, Faculty of Engineering and Environment, Northumbria University, Newcastle upon Tyne, UK;

[2] School of Earth and Environment, University of Leeds, Woodhouse Lane, Leeds, UK;

[3] Atmosphere and Ocean Research Institute, University of Tokyo, Kashiwa, Japan;

[4] British Geological Survey, Keyworth, Nottingham, UK;

[5] School of Mathematics, University of Leeds, Leeds, UK;

[6] Japan Agency for Marine-Earth Science and Technology, Yokohama, Japan;

[7] National Center for Atmospheric Research, Boulder, CO, USA;

[8] School of Geographical Sciences, University of Bristol, University Road, Bristol, UK;

[9] Columbia University - NASA/GISS, New York, NY, USA;

[10] LSCE/IPSL, CNRS-CEA-UVSQ, Saclay, France;

[11] Sisyphe, CNRS/UPMC Univ Paris 06, Paris, France;

[12] Eastern Geology and Paleoclimate Science Center, US Geological Survey, Reston, VA, USA;

[13] Graduate School of Life and Environmental Sciences, University of Tsukuba, Tsukuba, Japan;

[14] Alfred Wegener Institute for Polar and Marine Research, Bremerhaven, Germany;

[15] Institute of Atmospheric Physics, Chinese Academy of Sciences, Beijing, China;

[16] Bjerknes Centre for Climate Research, Bergen, Norway

* corresponding author:

Email: Ulrich.Salzmann@northumbria.ac.uk

Tel: Tel. +44 (0)191 2273874

**Uncertainties, bioclimatic ranges and temporal variability in proxy data and climate model outputs are often neglected in data-model comparisons designed to test the predictive ability of climate models, or differentiate between the performance of individual models within an ensemble. Here we use a global data set of confidence-assessed, proxy-based temperature estimates and biome reconstructions to assess the ability of eight models to simulate warm terrestrial climates of the Pliocene. The Late Pliocene, 3.6 to 2.6 million years ago, is an accessible geological interval to understand climate processes of a warmer world [1]. Here we show that model-predicted surface air temperatures reveal a substantial cold bias in the Northern Hemisphere. Particular strong data-model mismatches exist in Northern Russia where differences in mean annual temperatures reach 18 °C. Our model sensitivity tests identify insufficient temporal constraints hampering the accurate configuration of boundary conditions as an important factor impacting on data-model discrepancies. We conclude that in order to allow a more robust evaluation of the ability of current climate models to predict warm climates, future Pliocene data-model comparison studies must focus on orbitally defined time slices.**

Our understanding of causes and consequences of global warming relies heavily on climate model simulations conducted under a variety of greenhouse gas emission scenarios [2]. Comparing model simulations of key warm periods in Earth history with contemporaneous geological proxy data is one approach to evaluate the ability of these models to simulate warm, high $CO_2$-climates which are unprecedented in the more recent past. Existing data-model comparisons (DMCs) demonstrate that climate models are generally able to reproduce past warm climates of the last 65 million years [3-5]. However, a common data-model mismatch in high-latitude temperature estimates suggests that many models seem to underestimate polar amplification [4-6]. This has led to an ongoing controversy about the accuracy of DMC-studies, which might have been biased by uncertainties in estimating temperatures from geological proxies. Recently published proxy-based temperature reconstructions, suggesting tropical-like climates at southern high latitudes ca. 53 Myr ago [7], have intensified the ongoing debate and highlight the need of a systematic assessment in DMC-studies of uncertainty ranges and variability.

Here we compare Late Pliocene mean annual surface air temperature (SAT) estimates derived from 45 palaeobotanical sites with simulations of eight fully coupled ocean-atmosphere climate models (Fig. 1). All models have been initialised and run using an established experimental design and protocol, assuming an atmospheric $CO_2$-concentration of 405 ppmv [8]. From a data perspective our comparison includes the bioclimatic range, temporal variability, a new qualitative assessment of confidence in temperature estimates, and biome reconstructions. For the climate modelling, we consider inter-model differences in temperature predictions, as well as sensitivity to varying boundary conditions such as orbital parameters, atmospheric $CO_2$-concentrations and prescribed vegetation cover. The additional use of the BIOME4 classification scheme [9, 10] allows a direct comparison between palaeobotanical data and model outputs and therefore reduces potential complicating factors produced by different methods applied to derive temperature estimates from the fossil record. We compare global biome predictions from two selected models and with medium (HadCM3) and high (MIROC4m) climate sensitivity [11, 15].

## Multi-model variability and proxy data uncertainties

The zonal averages from each of the eight models (Fig. 1) demonstrate how the models within the ensemble have influenced the multi-model mean (MMM) zonal average. The MIROC4m and COSMOS models show the strongest SAT response in the ensemble (Fig. 1; $\Delta SAT_{\_global}$ 3.46 – 3.60). In terms of the global annual mean SAT anomaly, CCSM4 and MRI show the weakest SAT response to the implementation of Pliocene boundary conditions ($\Delta SAT_{\_global}$: 1.9 and 1.8 respectively). These results are generally consistent with the spread of climate sensitivity values for the eight models (Supplementary Table S1) which is highest for MIROC4m (4.05 °C) and COSMOS (4.1 °C) and between 2.7 °C and 3.2 °C for all other models. An energy balance analysis shows that the models with the highest temperatures in the Northern Hemisphere high latitudes, and the highest overall climate sensitivity, exhibit enhanced Arctic feedbacks (Supplementary Fig. S2). Conversely the models (CCSM4 and MRI) with the least polar amplification have suppressed Arctic feedbacks and fail to reproduce a sea-ice free Arctic summer.

If available, we included for our data-model comparison for each palaeobotanical site (Supplementary Table S3) the 1) "bioclimatic range", which is the temperature range under which the reconstructed palaeoflora existed, as derived from modern plant assemblage relationships (Fig. 3d, Supplementary Fig. S1), and 2) "temporal variability", which is the maximum minus the minimum temperature over the time recorded in the geological proxy (Fig. 3e). We have also combined "temporal variability" and "bioclimatic range" (see Supplementary Table S5 and Supplementary Section 6). Following guidance developed by the IPCC [12] we qualitatively assessed the level of "confidence" for each data site.

The Late Pliocene climate shows a generally lower temporal variability than the glacial and interglacials of the Quaternary, although a period of significant global cooling is recorded after ca. 3 Ma. [13]. We have addressed the possibility that this may have introduced a potential cool bias on our dataset, by using two global biome reconstructions from 205 palaeobotanical sites. The biome datasets reconstruct the global vegetation during colder/drier and warmer/wetter intervals within the Late Pliocene stage (Fig. 2). Biomes which remained relatively stable are the warm temperate forests (e.g. in Europe and Asia) as well as the woodlands and forests of central and southern Africa. Palaeobotanical sites which show fluctuations between cooler/drier and warmer/wetter biome types are typically situated near palaeogeographic transitions of major vegetation zones. This includes the northernmost Arctic records from North America which change from boreal forests to tundra shrubs, many sites in western North America which fluctuate between open conifer woodland and temperate xerophytic shrubland, and most palaeorecords from Japan that indicate changes from warm-temperate to slightly colder temperate deciduous forest biomes (Fig. 2). However, our assessment of biome temporal variability demonstrates that the vegetation changes between 3.6-2.6 million years were in many regions relatively minor compared to those of the Quaternary. The warm vegetation dataset predominantly shows the best fit for the majority of model simulations presented here (Supplementary Table S4).

**Comparison of Pliocene surface air temperatures from models and data**

The difference between model-simulated Pliocene and pre-industrial SATs shows increased temperatures in both hemispheres. The warming is particularly acute at high latitudes, north of the Arctic Circle and in regions of Antarctica where ice was removed in the climate model set-up (Fig. 3a). Proxy-based Pliocene SAT anomalies display a similar trend for the temperate and polar zones of the Northern Hemisphere (Fig. 3b). The few temperature estimates available for the Southern Hemisphere show no consistent large-scale pattern whilst tropical temperatures remained unchanged or experienced cooling during the Late Pliocene.

Point-by-point comparison of SAT anomalies indicate that the models do not sufficiently weaken the SAT gradient from the tropics to the high-latitudes because they underestimate the degree of SAT warming reconstructed by terrestrial proxies in the mid to high-latitudes of the Northern Hemisphere (Fig. 3c). This is particularly seen in Eurasia where temperature differences reach as much as 18°C. These temperature differences are derived from sites some of which have been assessed as 'high' or 'very high' confidence, and there is no evidence to assume a systematic bias in these estimates. The few temperature estimates available for the tropical zone tentatively suggest that the underestimation of SATs in the high latitudes may be accompanied by an overestimation in the low latitudes by 1- 6 °C (Fig. 3c). Recently identified sea surface temperature discrepancies between model predictions and proxy-data estimates in the North Atlantic[14] may be related to a cool bias in model predictions of European SATs identified in this study.

**The impact of boundary conditions on the model fit to data**

To further examine the potential causes of the identified data-model mismatches we explored the model sensitivity to imposed geological boundary and initial conditions by performing five additional simulations using HadCM3 and MIROC4m (Supplementary Table S2). Overall, the implementation of more recently developed boundary conditions [15, 16] (PRISM3 in Table 1, Supplementary Fig. S3) acts to reduce zonally averaged SATs in the Northern Hemisphere in comparison with the previously used data set (PRISM2 [17] in Table 1). This is likely to be a consequence of increased mountain height[19]. A DMC of ΔSATs for three selected palaeobotanical sites reveal that the implementation of PRISM3 boundary conditions results in a decrease of ΔSATs at the polar and temperate sites by ca. 3°C and 1°C, respectively, whilst at the tropical site ΔSATs increase slightly. In contrast to mean annual SATs, which indicate a greater data-model mismatch after the implementation of PRISM3 boundary conditions, the comparison of polar biomes using Kappa statistics indicate an improvement of model to data fit caused by a further northward extension of the boreal forests (Table 1). Biomes are integrators of climate change and their distribution is controlled by a range of additional climate parameters such as the length of growing season and annual rainfall. Whilst a smaller Greenland ice sheet in the new PRISM3 data set has only regional implications [18, 19], the introduction of a new vegetation cover and update of its physical parameters increased summer temperatures in the Northern Hemisphere resulting in a northward shift of boreal forests.

We also examined the sensitivity of HadCM3 and MIROC4m predictions to imposed orbital configuration and varying atmospheric $CO_2$-concentrations[20]. Our experiments suggest that orbital parameters which deliver the maximum degree of warmth at 65° N in summer improve the data-model fit for SATs at the high latitudes of the Northern Hemisphere (Table 1), where many of the mismatches occur for sites characterised as ‘high’ confidence. A further improvement can be achieved by increasing $CO_2$ concentration in the atmosphere to 450 ppmv, the maximum level suggested by proxy-$CO_2$ data [8]. However, these changes in boundary condition increase SATs at high as well as low latitudes resulting in a generally weaker data to model fit in the tropics in all models. The comparison of biome distribution shows that the best data-model fit is achieved under PRISM3 standard Pliocene boundary conditions in the HadCM3 and MIROC4m sensitivity experiments.

## Conclusion and Implication

Our DMC identifies a cold bias in models in the Northern Hemisphere (particularly north of 30 °N) demonstrating that, given the boundary conditions we have applied, none of the models used in this study reproduce the magnitude of northern hemisphere high-latitude warming exhibited in this proxy-dataset (Fig. 3c). A tentative data model mismatch may also be evident in the tropical zone where modelled Pliocene SATs appear to be too high, however this is limited by data availability.

Before drawing any conclusions with regard to the ability of climate models to reproduce the Pliocene, the potential causes of mismatches between palaeo-data and –models must be fully understood. Our DMC has identified regions (i.e. northern Russia, North Alaska and northeast Australia) where our data model mismatch is apparent when considering bioclimatic range (Fig. 3d), temporal variability (Fig. 3e) and even a combination of both factors (Fig. 3f). We have qualitatively assessed these sites as 'medium' to 'very high confidence'. The underlying reasons for these large DMC mismatches are still unknown.

Our DMC results also demonstrate that at many localities the spread in model-predicted SAT anomalies, from the model ensemble, is sufficiently large to cause an overlap with the available range of proxy-derived SAT anomalies (highlighted by the purple squares in Fig. 3g). At these localities it is possible to use the proxy data to differentiate between the performance of individual models. However, at this time such a differentiation would be difficult to complete accurately given the only partially quantified factors of bioclimatic range and temporal variability. For example, Figure 3e shows that out of the 14 data localities for which estimates of temporal variability are available, the MMM falls within the proxy-derived temperature range 43% of the time. The importance of temporal variability is also highlighted by comparison of biome simulations. Kappa scores (Table 1) for biome reconstructions indicate improved data to model fit with different orbital configurations is possible in a specific latitudinal band (e.g. polar), but often at the cost of a degraded model/data fit in other bands (i.e. the tropics and/or temperate). This is in line with the premise that the proxy data is not consistent with a single orbital configuration, rather the proxy records are representing multiple intervals of time through the mid-Pliocene, which were characterised by different orbital forcing and potentially atmospheric $CO_2$-concentration as well.

Our analysis shows that a tightly constrained time slice proxy reconstruction is necessary in order to reduce the importance of temporal variability in determining any assessment of the relative performance of models within an ensemble. A selection of a time slice [21] has the added advantage of making it possible to provide climate models with values for orbital forcing that are known to be consistent with a given proxy data reconstruction.

## Material and Methods

All climate modelling groups followed the Pliocene Model Intercomparison Project (PlioMIP) Experiment 2 design [15], using terrestrial boundary conditions from the "Pliocene Research, Interpretation and Synoptic Mapping" project PRISM [16]. Model specific details on the implementation of the mid-Pliocene boundary conditions, model spin-up and data-model comparison methods can be found in the Supplementary Information. We also incorporate additional Pliocene HadCM3 and MIROC4m sensitivity simulations that explore the effect of prescribing different boundary conditions, such as the effect of adjusting orbital parameters and/or the concentration of atmospheric carbon dioxide ($CO_2$), which provides either maximum hemispheric forcing and/or maximum potential $CO_2$-forcing.

Two independent methods for data-model comparison have been employed. In the first approach 45 quantitative temperature estimates from palaeobotanical proxies were used and compared to model predictions (Supplementary Table S3). Temperature estimates have been taken from literature or derived using the Coexistence Approach [22] and Palaeoflora Database [23]. If available, we took the author's interpretation from the original research paper to define climatic ranges for each temperature estimate. The confidence of each data set has been qualitatively assessed in regard to fossil preservation, temperature estimate methods, age control and resolution. Our model data comparison is necessarily qualitative because of the qualitative nature of the confidence assessments. In the second approach (forward modelling) biome reconstructions for the Late Pliocene from 205 palaeobotanical sites (Fig. 2) were compared with outputs of a mechanistically-based biome model (BIOME4; see Supplementary Information) forced by the HadCM3 and MIROC4m sensitivity simulations. BIOME4 model outputs and data have been quantitatively compared using kappa statistics [24]. Further details of the methodology of data synthesis and biome reconstruction are outlined in the Supplementary Information.

**Acknowledgements**

Financial support was provided by grants to U.S. and A.M.H. from the Natural Environment Research Council, NERC (NE/I016287/1). A.M.D. and A.M.H. acknowledge financial support from the European Research Council under the European Union's Seventh Framework Programme (FP7/2007-2013)/ERC grant agreement no. 278636. D.J.L. and F.J.B. acknowledge the NERC grant NE/H006273/1. U.S, A.M.D, H.J.D. and A.M.H thank the US Geological Survey John Wesley Powell Center for Analysis and Synthesis. W.-L.C and A.A.-O. acknowledge financial support from the Japan Society for the Promotion of Science and computing resources at the Earth Simulator Center, JAMSTEC. H.J.D. acknowledges the continued support of the US Geological Survey Climate and Land Use Change Research and Development Program; D.J.H. acknowledges the Leverhulme Trust for the award of an

Early Career Fellowship and the National Centre for Atmospheric Research and the British Geological Survey for financial support. G. L. received funding through the Helmholtz research programme PACES and the Helmholtz Climate Initiative REKLIM. C. S. acknowledges financial support from the Helmholtz Graduate School for Polar and Marine Research and from REKLIM. B.O-B. and N.A.R. recognize the National Center for Atmospheric Research is sponsored by the US National Science Foundation and computing resources were provided by the Climate Simulation Laboratory at the National Center for Atmospheric Research's Computational and Information Systems Laboratory sponsored by the National Science Foundation and other agencies.

## Authors Contributions

U.S. synthesised the palaeobotanical proxy data and designed and completed the confidence assessments. U.S., M.J.P., J.V. and H.J.D. carried out the data-model comparisons. A.M.D. and A.M.H. carried out the comparisons of model performance and the BIOME4 simulations. W.-L. C. performed the additional sensitivity experiments using MIROC. D.J.H carried out the energy balance analysis. All other authors performed general circulation model simulations which contributed to the PlioMIP Project and discussed the results and commented on the manuscript.

## Additional information

The authors declare no competing financial interests. Supplementary information accompanies this paper on www.nature.com/natureclimatechange. Reprints and permissions information is available online at www.nature.com/reprints. Correspondence and requests for materials should be addressed to U.S.

## References

1. Jansen, E., *et al*. in *Climate Change 2007: The Physical Science Basis. Contribution of Working Group I to the Fourth Assessment Report of the Intergovernmental Panel on Climate Change* (eds.

Solomon, S., Qin, D., Manning, M., Chen, Z., Marquis, M., Averyt, K.B., Tignor, M. & Miller, H.L.) 433–497. (Cambridge Univ. Press, Cambridge, 2007).

2. Randall, D.A., *et al*. in *Climate Change 2007: The Physical Science Basis. Contribution of Working Group I to the Fourth Assessment Report of the Intergovernmental Panel on Climate Change* (eds. Solomon, S., Qin, D., Manning, M., Chen, Z., Marquis, M., Averyt, K.B., Tignor, M. & Miller, H.L.) 589–662. (Cambridge Univ. Press, Cambridge, 2007).

3. Masson-Delmotte, V., et al. Past and future polar amplification of climate change: climate model intercomparisons and ice-core constraints. *Clim. Dynam*. **26**, 513-529 (2006).

4. Salzmann, U., Haywood, A.M., Lunt, D.J., Valdes, P.J. & Hill, D.J. A new global biome reconstruction and data-model comparison for the Middle Pliocene. *Global Ecol. Biogeogr*. **17**, 432-447 (2008).

5. Shellito, C. J., Lamarque, J.-F. & Sloan, L. C. Early Eocene Arctic climate sensitivity to pCO2 and basin geography. *Geophys. Res. Lett*. **36**, L09707 (2009).

6. Huber, M. & Caballero, R. The early Eocene equable climate problem revisited, *Clim. Past* **7**, 603-633 (2011).

7. Bijl, P.K., *et al*. Early Palaeogene temperature evolution of the southwest Pacific Ocean. *Nature* **461**, 776-779 (2009).

8. Pagani, M., Liu, Z., LaRiviere, J., Ravelo, A.C. High Earth-system climate sensitivity determined from Pliocene carbon dioxide concentrations. *Nature Geosci.* **3**, 27–30 (2010).

9. Prentice, I.C., *et al*. A global biome model based on plant physiology and dominance, soil properties and climate. *J. Biogeogr.* **19**, 117–134 (1992).

10. Kaplan, J. O., *et al.* Climate change and arctic ecosystems II: modeling, paleodata-model comparisons, and future projections. *J. Geophys. Res. Atmos.* **108**, 8171 (2003).

11. Hansen, J. et al. in *Climate Processes and Climate Sensitivity* (eds Hansen, J. E. & Takahashi, T.) 130-163 (American Geophysical Union, 1984).

12. Mastrandrea, M.D., *et al. Guidance Note for Lead Authors of the IPCC Fifth Assessment Report on Consistent Treatment of Uncertainties*. Intergovernmental Panel on Climate Change (IPCC). Available at http://www.ipcc.ch (2010).

13. McKay, R., *et al.* Antarctic and Southern Ocean influences on Late Pliocene global cooling . *PNAS* **109**, 17, 6423-6428 (2012).

14. Dowsett, H.J., *et al*. Assessing confidence in Pliocene sea surface temperatures to evaluate predictive models. *Nature Clim. Change* **2**, 365-371 (2012).

15. Haywood, A.M., *et al.* Pliocene Model Intercomparison Project (PlioMIP): Experimental design and boundary conditions (Experiment2). *Geosci. Model Dev.* **4**, 571-577 (2011).

16. Dowsett, H., *et al*. The PRISM3D Paleoenvironmental Reconstruction. *Stratigraphy*, **7**, 123-139 (2010).

17. Dowsett, H.J. *et al*. Middle Pliocene paleoenvironmental reconstruction: PRISM2. *USGS Open File Report*, **99-**535(1999).

18. Lunt, D.J., Foster, G.L., Haywood, A.M. & Stone, E.J. Late Pliocene Greenland glaciation controlled by a decline in atmospheric $CO_2$ levels. *Nature* **454**, 1102-1106 (2008).

19. Lunt, D.J., *et al.* On the causes of mid-Pliocene warmth and polar amplification. *Earth Planet. Sc. Lett.* **321-322**, 128-138 (2012).

20. Lisiecki, L.E. & Raymo, M.E. A Pliocene-Pleistocene stack of globally distributed benthic $^{18}O$ records. *Paleoceanography* **20**, PA1003 (2005).

21. Haywood, A.M., *et al*. On the identification of a Pliocene time slice for data-model comparison. *Phil.Trans.Roy.Soc.A*. (in press).

22. Mosbrugger, V. & Utescher, T. The coexistence approach – a method for quantitative reconstructions of Tertiary terrestrial palaeoclimate data using plant fossils. *Paleogeogr. Palaeoclimatol. Palaeoecol.* **134**, 61–86 (1997).

23. Utescher, T. Mosbrugger, V. Palaeoflora Database. Available at http://www.palaeoflora.de (2010).

24. Salzmann, U., Haywood, A.M. & Lunt, D.J. The past is a guide to the future? Comparing Middle Pliocene vegetation with predicted biome distributions for the twenty-first century. *Phil. Trans. Roy. Soc. A.* **367**, 189–204 (2009).

25. Cohen, J. A coefficient of agreement for nominal scales. *Educ. Psychol. Meas.* **2**, 37–46 (1960).

26. Legates, D.R., & Willmott, C.J. Mean seasonal and spatial variability in global surface air temperature. *Theor. Appl. Climatol.* **41**, 11-21 (1990).

27. Harrison, S.P. & Prentice, I.C. Climate and $CO_2$ controls on global vegetation distribution at the last glacial maximum: analysis based on palaeovegetation data, biome modelling and palaeoclimate simulations. *Glob. Change Biol.* **9**, 983–1004 (2003).

## Figure Legends

Figure 1: **Zonally averaged mean annual surface air temperatures (SAT) in °C**. Plotted zonally averaged SATs from modern observations, the multi-model mean prediction for the pre-industrial era and the Pliocene multi-model mean. Individual Pliocene zonal means are shown for all eight models.

Figure 2: **Location of 208 palaeobotanical sites used for data-model comparisons**. Rectangles indicate sites with sufficient resolution and dating control to reconstruct biomes for cold/dry (upper square) and warm/wet (lower square) climate periods or cycles. Circle colour indicates reconstructed biomes for other sites. Red square highlights 45 palaeo sites with temperature estimates used in this study (see Supplementary Table S3 and S4).

Figure 3: **Data-model comparison of global temperature estimates**. a) multi-model mean (MMM) SAT anomaly (°C) (Pliocene minus pre-industrial). 3b) proxy-based Pliocene

SAT anomalies (Pliocene absolute SATs minus observed SATs from Legates and Wilmott[26]). 3c) difference between MMM SAT anomaly and proxy-based Pliocene SAT anomalies. 3d) the degree of remaining data-model mismatch, when the known bioclimatic range, 3e) temporal variability and 3f) the climatic range are taken into account. Green circles (3d-3f) indicate where the MMM sits within the range of data. 3g) Purple squares show where at least one model in the ensemble fits within the available range of data at each site (see Supplementary Information).

## Tables

Table 1: **Data-model comparison for BIOME4 HadCM3 (PRISM2 and PRISM3) and MIROC (PRISM3)** . Table shows DMC results for annual SATs using regression analysis ($R^2$), differences in modelled and poxy-based SATs (model minus data) for three selected sites and difference between model and proxy-based mega-biome reconstructions [27] using a warm biased dataset. Kappa values [26] (κ) for global, polar, temperate tropical zones are ranked using a subjective assessment scale, whereby "0" means that the agreement is no better than would be expected by chance and "1" stands for a perfect match.

| Model | $R^2$ (SAT) | Δ°C SAT Model - Data | | | Kappa Values | | | |
|---|---|---|---|---|---|---|---|---|
| | | 55.7°N L. Baikal | 33.1°N C. Kyushu | 17.4 °S Butcher Cr. | Global | Polar > 60° N | Temperate 60°-23.5° | Tropic <23.5° N/S |
| **Pliocene HadCM3 PRISM2** | **0.85** | -8.73 | 2.76 | 4.98 | **0.31** | 0.01 | 0.29 | 0.03 |
| NH Max Orbit | 0.87 | -7.97 | 2.21 | 5.23 | **0.28** | 0.30 | 0.17 | 0.19 |
| SH Max Orbit | 0.85 | -8.90 | 3.10 | 4.93 | **0.30** | 0.00 | 0.26 | 0.11 |
| NH Max Orbit $CO_2$ 450 ppm | 0.87 | -7.33 | 2.67 | 5.47 | **0.31** | 0.42 | 0.21 | 0.15 |
| SH Max Orbit $CO_2$ 450 ppm | 0.85 | -8.08 | 3.20 | 5.11 | **0.33** | 0.03 | 0.26 | 0.16 |
| **Pliocene HadCM3 PRISM3** | **0.83** | -11.81 | 1.81 | 5.32 | **0.30** | 0.41 | 0.23 | 0.00 |
| NH Max Orbit | 0.84 | -10.28 | 0.53 | 6.05 | **0.25** | 0.24 | 0.17 | 0.14 |
| SH Max Orbit | 0.83 | -10.62 | 3.20 | 5.62 | **0.30** | 0.23 | 0.25 | 0.05 |
| NH Max Orbit $CO_2$ 450 ppm | 0.84 | -9.74 | 1.18 | 6.41 | **0.22** | 0.20 | 0.14 | 0.09 |
| SH Max Orbit $CO_2$ 450 ppm | 0.83 | -9.99 | 3.55 | 5.97 | **0.30** | 0.35 | 0.24 | 0.03 |
| **Pliocene MIROC PRISM3** | **0.83** | -10.52 | 1.91 | 6.45 | **0.30** | 0.36 | 0.21 | 0.06 |
| NH Max Orbit | 0.84 | -9.22 | 1.62 | 6.73 | **0.26** | 0.17 | 0.21 | 0.12 |
| SH Max Orbit | 0.83 | -10.87 | 2.31 | 6.35 | **0.29** | 0.15 | 0.21 | 0.06 |
| NH Max Orbit $CO_2$ 450 ppm | 0.84 | -8.59 | 2.08 | 7.09 | **0.25** | 0.12 | 0.22 | 0.11 |
| SH Max Orbit $CO_2$ 450 ppm | 0.83 | -9.69 | 2.82 | 7.21 | **0.29** | 0.30 | 0.20 | 0.06 |

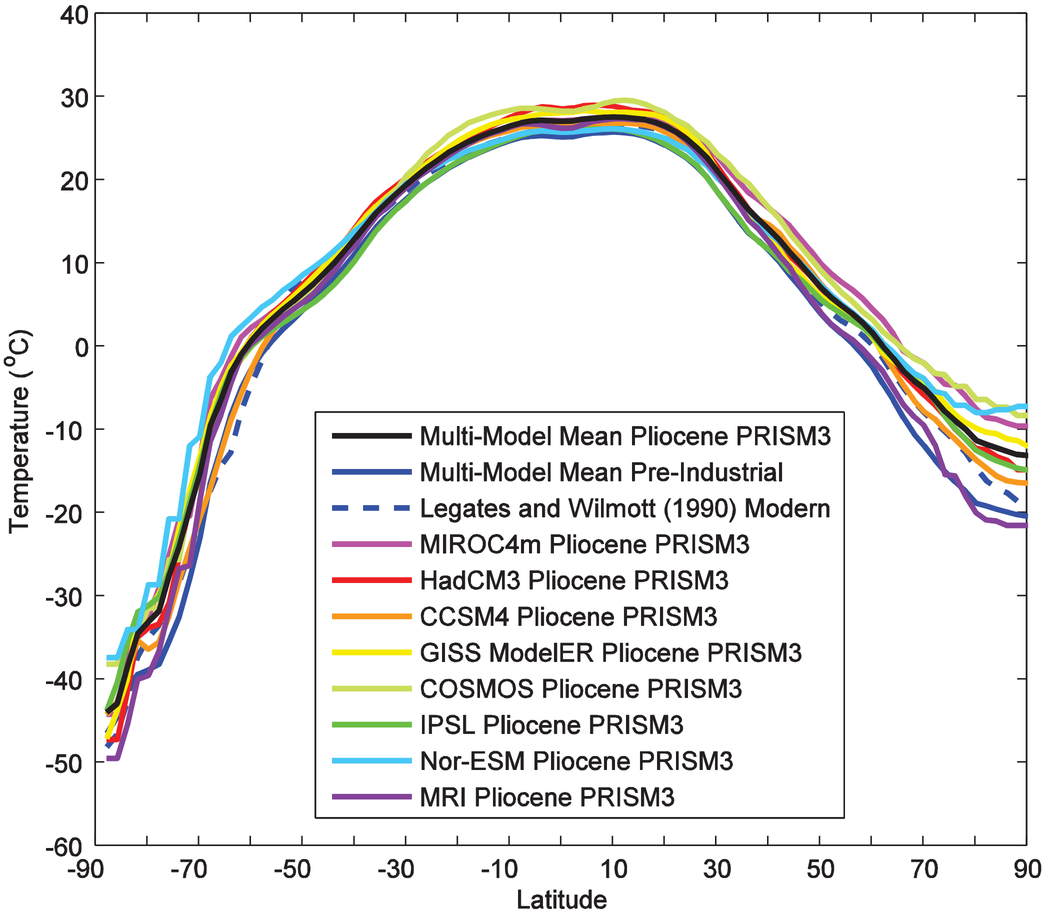


Figure 1: **Zonally averaged mean annual surface air temperatures (SAT) in °C**

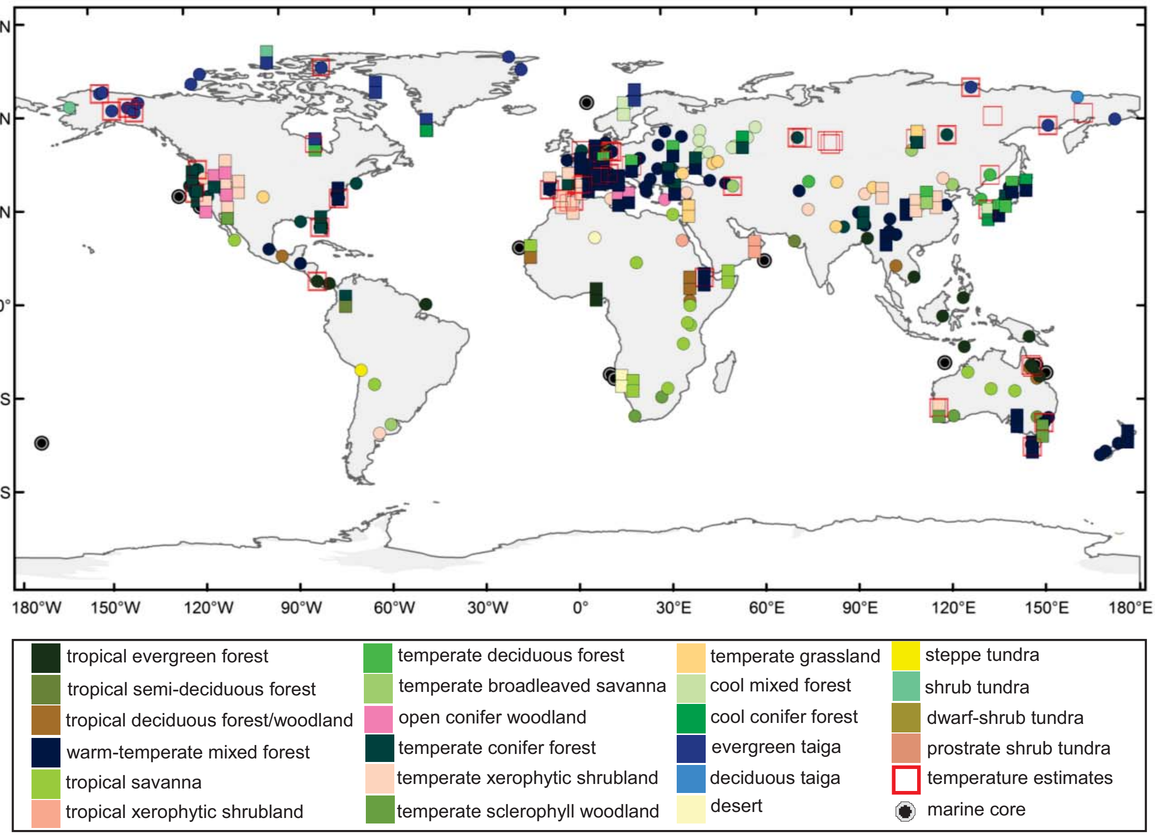


Figure 2: **Location of 208 palaeobotanical sites used for data-model comparisons**

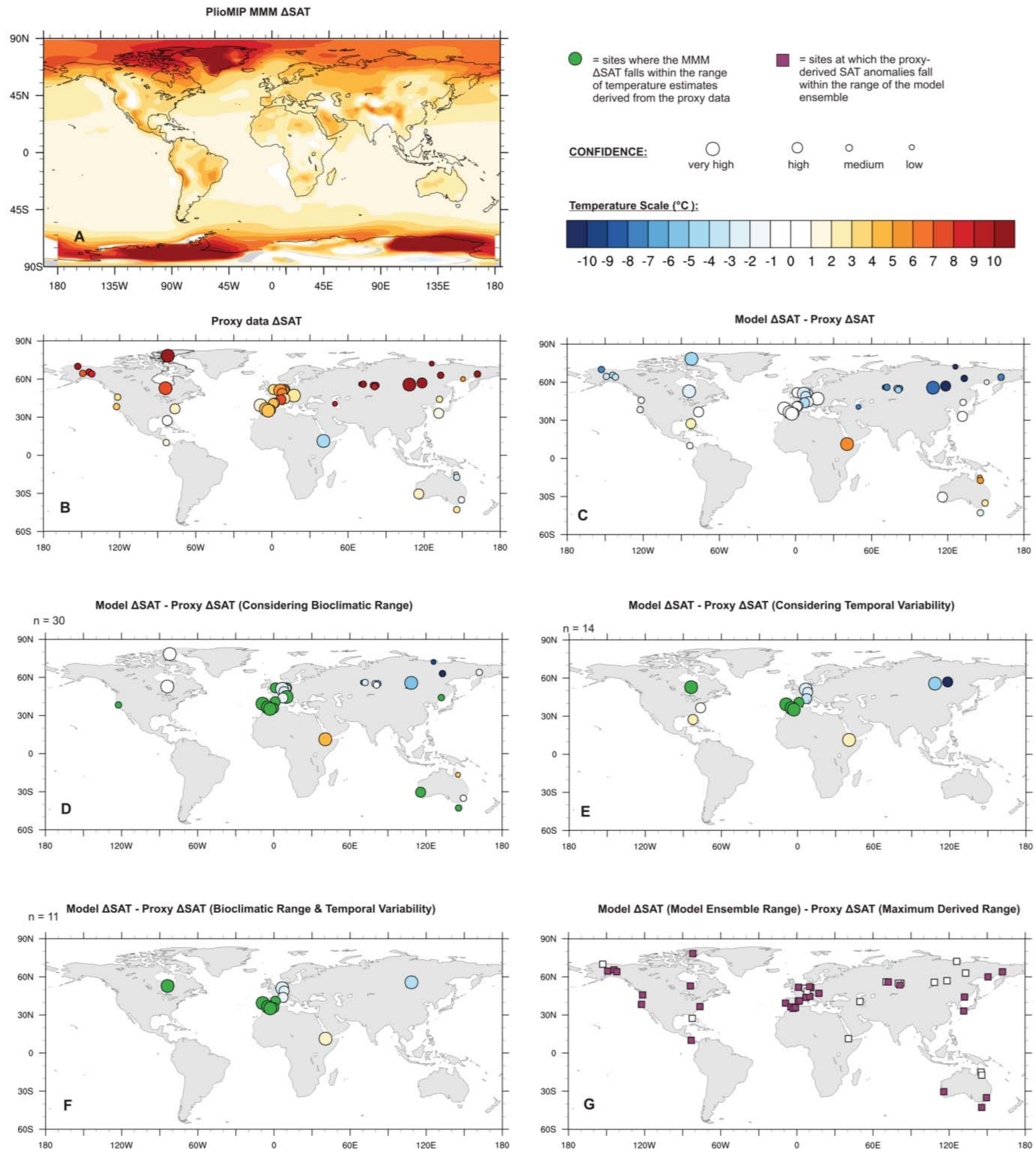


Figure 3: **Data-model comparison of global temperature estimates.**

# Supporting Information for:

# Data-model discord reveals challenges in reconstructing terrestrial warming of the Pliocene

Ulrich Salzmann[1*], Aisling M. Dolan[2], Alan M. Haywood[2], Wing-Le Chan[3], Daniel J. Hill[4], Jochen Voss[5], Ayako Abe-Ouchi[3,6], Bette Otto-Bliesner[7], Fran Bragg[8], Mark A. Chandler[9], Camille Contoux[10,11], Harry J. Dowsett[12], Anne Jost[11], Youichi Kamae[13], Gerrit Lohmann[14], Daniel J. Lunt[8], Steven J. Pickering[2], Matthew J. Pound[1], Gilles Ramstein[10], Nan A. Rosenbloom[7], Linda Sohl[9], Christian Stepanek[14], Hiroaki Ueda[13], Zhongshi Zhang[15,16]

[1] Department of Geography, Faculty of Engineering and Environment, Northumbria University, Newcastle upon Tyne, UK; [2] School of Earth and Environment, University of Leeds, Woodhouse Lane, Leeds, UK; [3] Atmosphere and Ocean Research Institute, University of Tokyo, Kashiwa, Japan; [4] British Geological Survey, Keyworth, Nottingham, UK; [5]School of Mathematics, University of Leeds, Leeds, UK; [6] Japan Agency for Marine-Earth Science and Technology, Yokohama, Japan; [7] National Center for Atmospheric Research, Boulder, CO, USA; [8] School of Geographical Sciences, University of Bristol, University Road, Bristol, UK; [9] Columbia University - NASA/GISS, New York, NY, USA; [10] LSCE/IPSL, CNRS-CEA-UVSQ, Saclay, France; [11] Sisyphe, CNRS/UPMC Univ Paris 06, Paris, France; [12] Eastern Geology and Paleoclimate Science Center, US Geological Survey, Reston, VA, USA; [13] Graduate School of Life and Environmental Sciences, University of Tsukuba, Tsukuba, Japan; [14] Alfred Wegener Institute for Polar and Marine Research, Bremerhaven, Germany; [15]Institute of Atmospheric Physics, Chinese Academy of Sciences, Beijing, China; [16]Bjerknes Centre for Climate Research, Bergen, Norway

## 1. Description of climate models and outputs

Pliocene climate model runs (Supplementary Table S1) were initialised following the protocol of the Pliocene Modeling Intercomparison Project (PlioMIP), which incorporates the latest version of the US Geological Survey PRISM data set of boundary conditions (PRISM3) [1, 2] . Following this experimental design, atmospheric carbon dioxide was set to 405 ppmv in all of the climate model simulations. However, due to the lack of geological proxy data that can be used to robustly estimate methane

($CH_4$) and other trace gasses, dust emissions and aerosols for the Late Pliocene, these boundary conditions were left unchanged from pre-industrial conditions. Therefore a caveat associated with this experimental design is that the incorrect specification of these trace gasses, aerosols and dust emissions for the late Pliocene, may over- (or under-) estimate the degree of data model discord.

Simulated Pliocene surface air temperatures (SATs) were derived from the final 30 years of each model run and re-gridded on a standard 2°×2° lat/long grid to facilitate the production of a multi-model mean (MMM). The MMM has been calculated by taking an average of the eight models (detailed in Supplementary Table S1); HadCM3, MIROC4m, CCSM4, GISS Model ER, COSMOS, IPSLCM5A, MRI-GCM 2.3, NorESM-L. No model weighting has been applied in the creation of the MMM. Model ensemble means for the Southern Hemisphere higher than 50 degrees south are not considered reliable because of inconsistencies in the prescribed land/sea mask between the eight models (Supplementary Table S1).

**2. Description of BIOME4 vegetation model**

BIOME4 is a development of the BIOME3 model [3]. It is a coupled carbon and water flux model, which predicts global steady state vegetation distribution, structure and biogeochemistry. BIOME4 was developed from the physiological constraints influencing the distribution of different plant functional types (PFT). Twelve plant functional (PFT) types, each with a very specific range of bioclimatic limits, are represented in BIOME4, ranging from Arctic to tropical flora. BIOME4 determines which of 28 biomes is most likely to occur in a grid square based on computed biogeochemical variables [3, 4].

The model is forced by long-term averages of monthly mean temperature, precipitation and sunshine. Atmospheric carbon dioxide concentrations must be specified and information on soil texture and depth must also be provided. To force the vegetation model, a standard anomaly method is employed (as in [5-7]). This takes into account the systematic error in the climate model relative to present-day observations of climate [8]. Owing to the lack of sufficient observational data over

Antarctica, the anomaly method cannot be employed in this region and there, the absolute values from the climate model are used to force BIOME4.

**3. Sensitivity experiments**

To examine the potential bias that orbital and $CO_2$ forcing could introduce, orbital parameters and $CO_2$ levels were changed in a suite of HadCM3 and MIROC4m sensitivity experiments (see Supplementary Table S2). Orbital parameters were set to deliver the maximum amount of incoming solar radiation at the top of the atmosphere at specific latitudes (either 65°N for the Northern Hemisphere or 80°S for the Southern Hemisphere) during summer within the Pliocene. The orbital configuration in the HadCM3 sensitivity experiments is thus representative of time points in the Pliocene where extremes in summer insolation were shown in the astronomical solution of Laskar et al. [9]. The values of eccentricity, precession and obliquity are shown for reference in Supplementary Table S2. In some sensitivity experiments, $CO_2$ levels were also increased to 450 ppmv (from the standard PRISM3 value of 405 ppmv) to assess the impact on our data-model comparison (DMC) of specifying a higher level of $CO_2$ (thus promoting more climate warming). Late Pliocene atmospheric $CO_2$ concentrations of 450 ppmv are the maximum level suggested by proxy-$CO_2$ data [10].

In contrast to the previous iteration of the boundary condition data set (PRISM2), PRISM3 which was used in the PlioMIP protocol, specifies the height of the western cordillera of both North and South America to be at approximately modern altitude (in contrast to a 50% reduction in PRISM2). There are also substantial changes in the vegetation scheme used and in the distribution of ice on Greenland and Antarctica. Experiments using HadCM3, where the model boundary conditions were changed from PRISM2 to PRISM3, highlight the combined effect of changes in land surface on climate diagnostics such as SAT and biome type.

**4. Palaeobotanical dataset and temperature estimates**

We used an updated version of the Late Pliocene (3.6-2.6 Ma) palaeobotanical TEVIS dataset[11]. The dataset integrates marine and terrestrial vegetation data derived from fossil pollen, leaves, wood and palaeosol carbonate, whereby the authors' interpretation of palaeobotanical data, taken from the original research papers, was used and translated into the 28-type land-cover classification scheme of BIOME4 [12]. For the updated version presented here, we removed from the original dataset two re-dated sites from the Tjoernes Section in Iceland [12] and Sirius Group, Antarctica [13] and added data from 9 sites in Canada[14], Mexico [15], Russia [16, 17], Germany [18, 19], France [20], Portugal [21] and Turkey [22].

Uncertainties in estimating Pliocene palaeo-altitudes and locating the source of proxy data can significantly bias comparisons of temperature estimates. We therefore excluded terrestrial information from marine sites more than 250 km away from the mainland and estimates for sites with a modern altitude above 1000 m a.s.l. with the exception of one site for which temperatures have been adjusted to sea level by the original authors (Supplementary Table S3).

## 5. Assessing range and confidence of proxy data-based temperature estimates

Here, we discuss the various sources of uncertainty in our proxy temperature estimates. These are associated with temporal variability, bioclimatic range and additional unquantifiable uncertainties. We also discuss the process we use for assessing a qualitative indicator of our confidence in each data point.

### 5.1 Bioclimatic range and temporal variability

The bioclimatic range of a temperature estimate was derived (where available) from the fossil record using quantitative and semi-quantitative methods such as:

a) Climate Leaf Analysis Multivariate Program (CLAMP) [23] which uses the physiognomy of fossil leaves to determine past climates

b) Coexistence Approach (CA) [24], which uses the climatic requirements of the Nearest Living Relative (NLR) of fossil taxa to reconstruct the past climatic range (Supplementary Figure S1a)

c) Semi-quantitative methods using the climatic range of the nearest modern analogue vegetation distribution

d) Multi-proxy measurements that combine the above listed palaeobotanical methods with other palaeoclimate proxies, such as oxygen isotopes.

In our DMC study we either used published temperature estimates or, if not available, we applied the Coexistence Approach to generate temperature estimates from the fossil record (Supplementary Table S3). The quantitative and semi-quantitative temperature estimate techniques generally produce a temperature range rather than one absolute value (see Supplementary Figure S1a/b). Such ranges represent the climate interval in which all taxa of reconstructed palaeovegetation can co-exist. The bioclimatic range has a lower and upper limit of tolerance beyond which the nearest living relatives of the fossil assemblage cannot exist.

In addition to the bioclimatic range, we also included the temporal variability of a temperature estimate (Supplementary Figure S1b) in our DMC (where available). This takes into account the variability of the reconstructed vegetation in response to climate change over the time period covered by the fossil record (e.g. orbitally controlled cold and warm cycles). By including the temporal variability into our DMC we addressed uncertainties in age determination of the fossil record. However, it should be noted that depending on the quality and temporal resolution of the fossil record, temporal variability and bioclimatic ranges are not available for all sites. Generally, such sites have been assigned lower confidence levels (see also following sections).

### 5.2 Assessing the qualitative confidence of a temperature estimate

The quality of geological archives can strongly vary between sites and depends on a number of external factors, such as taphonomy, sedimentation rate, depositional environment and availability of datable material. These factors often impact on the quality of the proxy data and their use for environmental reconstruction. In order to address the variation in quality associated with our temperature estimates, we qualitatively assessed the level of confidence for each data point

(Supplementary Table S3). The criteria used to assign each data point to one of the four confidence levels (very high, high, medium and low) were: a) age control, b) resolution, c) fossil preservation and d) temperature estimate methods used. Temperature estimate methods and age control were the most important parameters impacting on the confidence levels of proxy data. Established quantitative methods have a generally higher confidence than semi-quantitative estimates using nearest living relatives. Temperature estimates with the highest confidence level are (i) typically well dated, using for example, radiometric or oxygen isotope dating methods, (ii) show an excellent fossil preservation that allows multi-proxy analyses, (iii) use quantitative methods such as CA or CLAMP and (iv) have a high resolution which allows the reconstruction of Late Pliocene mean annual temperature changes over several cold and warm cycles. Temperature estimates with a medium to low confidence typically have a poorer age control, which for example, is based on relative dating using similarities of fossil assemblages; (i) have a low diversity related to poor fossil preservation and (ii) use semi-quantitative temperature estimation techniques. The confidence level should be used in addition to the indicated temperature range as a guide to assess the robustness of a temperature estimate (see Fig. 3). Temperature estimates from sites with a high confidence level might be more accurate and reliable than other fossil records with lower confidence. However, we found a very good consistency between temperature estimates derived from high and lower confidence sites, in particular in high latitude Northeast Asia and North America (see Fig. 3b), indicating that impact of the level of confidence on DMC results appears to be rather low.

### 5.3 Additional unquantifiable uncertainties

Our DMC study focuses on two quantifiable sources of total uncertainty; bioclimatic range and temporal variability, because we consider that these are likely to have the largest impact on the total uncertainty of proxy temperature estimations. However, there are additional uncertainties in data and model derived temperature estimates which could potentially impact on the DMC results, but which are unquantifiable.

One additional uncertainty is caused by the fact that a model produces an average temperature over the size of one model grid cell, whereas data is collected from a single point in space. However, we consider this to have a rather small impact on the uncertainty ranges if compared to the temporal and bioclimatic ranges described above. Grid cell uncertainties gain importance in high altitude regions. However, most of our palaeobotanical sites are at altitudes below 350 m.a.s.l. (see Table S3) and we excluded any data points from our data set with a modern altitude above 1000 m. a.s.l. If we assume a) a Pliocene latitudinal temperature gradient of ca. 0.6 °C per degree in latitude[25] and b) that we further reduced uncertainties by using interpolation to the exact proxy location within the model grid cell and c) that the variation within the grid cell is also further reduced by the fact that our proxy based temperatures were derived from the predominant vegetation covering a wider area of the grid cell, then we have no reasons to assume that the uncertainty imposed by the size of a 2° x 2° grid cells exceeds 1°C.

Other additional uncertainties, such as methodological errors, might have a higher impact on the DMC results, although their uncertainties can hardly be quantified and vary between sites and methods applied. For example, CLAMP shows a tendency to produce for the Neogene temperature estimates that are generally colder (likely range 1-2°C) than CA[18]. The accuracy of the CA estimates, which is highest for temperature-related parameters and has been indicated to be usually in the range of 1–2 °C[26], has been recently questioned by a study[27], which identified remarkable inaccuracies in temperature reconstruction of warmer lowland and cooler vegetation at higher elevations. We therefore excluded any data points from our data set with a modern altitude above 1000 m. a.s.l.

**6. Performing a data-model comparison on surface air temperature**

To illustrate the differences between each model in the PlioMIP ensemble, zonal means were calculated by averaging the individual models across latitudinal bands (Fig. 1). The multi-model zonal mean is also shown on Fig. 1.

In order to compare MMM-predicted with proxy-based estimates of SAT both the modelled absolute temperatures (Table 1) and the modelled temperature anomalies from pre-industrial have been used (Fig. 3). Initially a visual comparison between the SAT anomalies was undertaken (Fig. 3c). Modelled temperature anomalies from the nearest grid square to the location of the proxy-data site were compared to data-based SATs (anomalies calculated to the Legates and Wilmott modern observational dataset[28]) in order to determine the spatial differences or similarities between the data-based and modelled anomalies.

The match between the absolute SAT data and the modelled SATs were evaluated in terms of their correlation using a simple linear regression ($r^2$; Table 1). It should be noted that this metric does not take into account any uncertainties in the proxies, and as such it should be interpreted with caution. Furthermore, statistical comparisons of absolute data and modelled SATs can be biased by the overriding effect of latitude on SAT, which can lead to a misleading level of agreement between the models and data. Therefore, testing the commonality between the SAT anomalies (mid-Pliocene minus modern/pre-industrial) produced by the model and the data provide a fairer test of the model [29]. For all panels in Figure 3, the SAT anomalies of the proxy-data and model have been used.

In Figures 3d and 3e, we show the impact on the DMC when we consider the proxy-derived bioclimatic range (available at 30 sites) and temporal variability (available at 14 sites). We demonstrate (using green circles) sites at which the MMM SAT anomaly falls within the range associated with the proxy data. Where both ranges are available (11 sites), we combine the bioclimatic range and temporal variability to create a total "climatic range" ($r_{total}$). From any given fossil sample only a range of possible values of the SAT can be determined and there is a deviation ($X_{bc}$) between true SAT and the center of the range of possible temperatures. This deviation represents a form of measurement error and the magnitude of $X_{bc}$ is described by the bioclimatic range $r_{bc}$. Similarly, the mean temperature fluctuates over the time period covered by the fossil record and at a given time there will be a deviation ($X_{tv}$) between the current mean temperature and the long term average of the SAT. The magnitude of $X_{tv}$ is described by the temporal variability $r_{tv}$. Using this notation, the true SAT at a given time and location can be described as the value reported in the SAT column of Supplementary Table S3b, plus $X_{bc} + X_{tv}$. Since $X_{bc}$ describes the position of the actual temperature within the range of temperatures allowed by the fossil record, whereas $X_{tv}$ is determined by the point in time an observation belongs to, it is reasonable to assume that both quantities are random and independent.

The numerical values for $r_{bc}$ and $r_{tv}$could be interpreted in different ways. The values could either be seen as hard limits for the corresponding temperature range (for example, the value of $r_{bc}$ could be interpreted to mean that we always have $-r_{bc} \leq X_{bc} \leq r_{bc}$), or as soft limits (for example, by assuming that the random value $X_{tv}$ satisfies $-r_{tv} \leq X_{tv} \leq r_{tv}$ with a given probability (e.g. $P(-r_{tv} \leq X_{tv} \leq r_{tv}) = 95\%$)). The same interpretations are possible for $r_{total}$. Similarly, different assumptions are possible for the distributions of the random values $X_{bc}$ and $X_{tv}$. In particular if the ranges are interpreted as hard limits, the random values could be assumed to be uniformly distributed on the range of possible values, or the distributions could be assumed to be more concentrated near the centre of the ranges (e.g. by assuming a normal distribution).

To represent the choices outlined above, we tested two different methods for combining the individual ranges into a single value. For the first method, we assume that $X_{bc}$ and $X_{tv}$ are independent and normally distributed with variances such that $P(-r_{bc} \leq X_{bc} \leq r_{bc}) = 95\%$ and $P(-r_{tv} \leq X_{tv} \leq r_{tv}) = 95\%$. In this case, the values $r_{bc}$ and $r_{tv}$ correspond to 1.96 standard deviations of $X_{bc}$ and $X_{tv}$, respectively, and the corresponding value for $r_{total}$ is given by:

$$r_{total} = \sqrt{r_{bc}^2 + r_{tv}^2}$$

This method seems the most natural approach (Supplementary Table S3b; Method 1). For the second method, we assume that $X_{bc}$ and $X_{tv}$ are uniformly distributed on the intervals $[-r_{bc}, r_{bc}]$ and $[-r_{tv}, r_{tv}]$ respectively. For easy comparison to the first method, we again choose $r_{total}$ to be the value such that $P(-r_{total} \leq X_{bc} + X_{tv} \leq r_{total}) = 95\%$ (Supplementary Table S3b; Method 2 (95%)). Since the probability of 95% in this approach was chosen rather arbitrarily, we also tested a variant of Method 2, where the probability 90% was used instead (Supplementary Table S3b, Method 2 (90%)). The resulting total ranges for the methods tested are very similar, and thus the method for combining $r_{bc}$ and $r_{tv}$ into a total range has little effect on the results. Therefore, in Figure 3f of our analysis, we use Method 1 described here to derive $r_{total}$ , and highlight sites where the MMM SAT anomaly falls within $r_{total}$ with green circles.

Figure 3g presents a summary of the data in Figures 3c to 3f and includes all proxy-data localities and the full range of SAT anomalies derived from the PlioMIP ensemble. Sites are coded as purple squares if any of the proxy-data available (both with and without ranges) falls within the model ensemble range. If this is the case, we argue that the data can be used as a means of discriminating between models within the ensemble. However, such an undertaking without knowledge of the magnitude of $r_{bc}$ and $r_{tv}$ would likely generate incorrect conclusions regarding individual model performance. White squares in Figure 3f demonstrate sites where the available proxy-data (i.e. with or without ranges) and the model ensemble do not overlap. One particular region where this occurs is in North East Asia/Siberia, which shows that the models are consistently too cold in comparison to the data.

**7. Performing a data-model comparison on biome reconstructions**

Global biome maps were compared numerically by employing the ArcView 3.x extension for kappa statistics [30]. The Kappa statistic measures the degree of agreement between predicted and observed categorisations of a dataset or map, while correcting for agreement that occurs by chance [31]. Kappa statistics have already been successfully applied for comparing Quaternary and Pliocene biome reconstructions [11, 32, 33]. Kappa values (κ) are ranked using a subjective assessment scale between 0 and 1, whereby "0" means that the agreement is no better than would be expected by chance and "1" stands for a perfect match. Kappa results strongly depend on the number of different classes selected and are rarely comparable across studies. Therefore, here we interpret our kappa values in isolation from previous studies [e.g. 7, 34]. For comparing biome reconstructions from fossil data with model simulations, we grouped the 28 biomes into broader units (mega-biomes[35]) to avoid the minimum number of sample points per category becoming too low for meaningful Kappa statistics.

### 8. PlioMIP Experiment 2 Energy Balance Analysis

By following the methods of Heinemann et al. [36] and Lunt et al. [37], we can model the energy balance components of each of the PlioMIP Experiment 2 simulations by approximating the temperature, T, at each latitude using the planetary albedo $\alpha$ , the effective longwave emissivity $\epsilon$ , and the implied net meridional heat transport divergence, H. Where $SW_{TOA}^{\downarrow}$ is the incoming shortwave radiation at the top of the atmosphere and $\sigma$ is the Stefan-Boltzmann constant,

$$T = \frac{\left(SW_{TOA}^{\downarrow}(1-\alpha) - H\right)^{1/4}}{\epsilon\sigma}$$

Due to their small changes relative to their absolute values, Pliocene warming can be approximated by a linear combination of changes in emissivity, albedo and heat transport. However, by assessing clear sky radiation components within the simulations, these components can be further broken down into the impact of changes in atmospheric greenhouse gases ($\Delta T_{gg\epsilon}$), cloud emissivity ($\Delta T_{c\epsilon}$), cloud albedo ($\Delta T_{c\alpha}$) and clear sky albedo ($\Delta T_{cs\alpha}$). At latitudes where changes in topography occur between the Pliocene and control simulations, the impact of these changes in surface altitude ($\Delta T_{topo}$) must also be accounted for. Therefore,

$$\Delta T_{Plio} = \Delta T_{gg\epsilon} + \Delta T_{c\epsilon} + \Delta T_{c\alpha} + \Delta T_{cs\alpha} + \Delta T_H + \Delta T_{topo}$$

The two simulations that show the greatest changes in the high latitudes of the Northern Hemisphere (MIROC and COSMOS) have the greatest climate sensitivity. Both also show the largest changes due to feedbacks in each of the albedo and emissivity components, even where the feedback is negative (Supplementary Figure S3). The complete loss of summer sea-ice and strength of Arctic feedbacks explain why these models show the greatest polar amplification of all the PlioMIP simulations (Supplementary Figure S4). Conversely CCSM and MRI show the least polar amplification, despite having climate sensitivities close to the best estimates of IPCC[38]. These simulations seem to have suppressed positive albedo feedbacks and, particularly in the case of MRI, enhanced negative feedbacks at key latitudes of the Northern Hemisphere.

## 9. References

1. Haywood, A.M., *et al.* Pliocene Model Intercomparison Project (PlioMIP): Experimental design and boundary conditions (Experiment2). *Geosci. Model Dev.* **4**, 571-577 (2011).

2. Dowsett, H., *et al*. The PRISM3D Paleoenvironmental Reconstruction. *Stratigraphy*, **7**, 123-139 (2010).

3. Kaplan, J.O. *Geophysical applications of vegetation modeling*. PhD thesis, Lund University, Lund (2001).

4. Kaplan, J.O. *et al.* Climate change and arctic ecosystems II: Modeling, paleodata-model comparisons, and future projections. *J. Geophys. Res.–Atmos.* **108**, 8171 (2003).

5. Haxeltine, A. & Prentice, I.C. BIOME3: An equilibrium terrestrial biosphere model based on ecophysiological constrains, resource availability, and competition among plant functional types. *Global Biogeochem. Cy.* **10**, 693-709 (1996).

6. Texier, D., *et al.* Quantifying the role of biosphere- atmosphere feedbacks in climate change: coupled model simulations for 6000 years BP and comparison with paleodata for northern Eurasia and Africa. *Clim. Dynam.* **13**, 865–882 (1997).

7. Salzmann, U., Haywood, A.M., & Lunt, D.J. The past is a guide to the future? Comparing Middle Pliocene vegetation with predicted biome distributions for the twenty-first century. *Phil. Trans. R. Soc. A* **367**, 189-204 (2009).

8. Leemans, R. & Cramer, W. The IIASA database for mean monthly values of temperature, precipitation and cloudiness of a global terrestrial grid. *International Institute for Applied Systems Analysis (IIASA)*. **RR-91-18** (1991).

9. Laskar, J. *et al.* A long-term numerical solution for the insolation quantities of the Earth. *Astron. Astrophys.* **428**, 261-285 (2004).

10. Pagani, M., Liu, Z., LaRiviere, J., Ravelo, A.C. High Earth-system climate sensitivity determined from Pliocene carbon dioxide concentrations. *Nature Geosci*. **3**, 27–30 (2010).

11. Salzmann, U., Haywood, A.M., Lunt, D.J., Valdes, P.J., Hill, D.J. A new global biome reconstruction and data-model comparison for the Middle Pliocene. *Global Ecol. Biogeogr.* **17**, 432-447 (2008).

12. Verhoeven, K., Louwye, S. Eiriksson, J. & De Schepper, S. A new age model for the Pliocene-Pleistocene Tjornes section on Iceland: Its implication for the timing of North Atlantic-Pacific palaeoceanographic pathways. *Palaeogeogr. Palaeoclimatol. Palaeoecol.* **309**, 33-52 (2011).

13. Wilson, G.S., *et al.* The Mount Feather Diamicton of the Sirius Group: an accumulation of indicators of Neogene Antarctic glacial and climatic history. *Palaeogeogr. Palaeoclimatol. Palaeoecol.* **182**, 117–131 (2002).

14. Gao, C., *et al.* Glaciation of North America in the James Bay Lowland, Canada, 3.5 Ma. *Geology* **40**,75-978 (2012).

15. Velasco-de León, M.P., Spicer, R.A. & Steart, D.C. Climatic reconstruction of two Pliocene floras from Mexico. *Palaeobiodivers. Palaeoenviron.* **90**, 99–110 (2010).

16. Blokhina, N. & Bondarenko, O. Woody plant assemblages and palaeoenvironments in the Pliocene of Pavlovskaya Depression (Southern Primory'e). *Acta Palaeontol. Rom.* **4**, 23-35 (2004).

17. Enikeev, F.I. The Late Cenozoic of northern Transbaikalia and paleoclimates of southern East Siberia. *Russ. Geol. Geophys.* **49**, 602-610 (2008).

18. Uhl, D., *et al*. Cenozoic paleotemperatures and leaf physiognomy: A European perspective. *Palaeogeogr. Palaeoclimatol. Palaeoecol.* **248**, 24-31 (2007).

19. Mai, D.H. The floral change in the Tertiary of the Rhön mountains (Germany). *Acta Palaeobot.* **47**, 135–143 (2007).

20. Teodoridis, V., Kvaček, Z. & Uhl, D. Late Neogene palaeoenvironment and correlation of the Sessenheim-Auenheim floral complex. *Palaeodiversity* **2**, 1-17 (2009).

21. Vieira M., Poças E., Pais J. & Pereira D. Pliocene flora from S. Pedro da Torre deposits (Minho, NW Portugal). *Geodiversitas* **33**, 71-85 (2011).

22. Yavuz-Isik, N. & Toprak, V. Palynostratigraphy and vegetation characteristics of Neogene continental deposits interbedded with the Cappadocia ignimbrites (Central Anatolia, Turkey). *Int. J.Earth Sci.* **99**, 1887-1897 (2010).

23. Wolfe, J.A. A method of obtaining climatic parameters from leaf assemblages. *U.S. Geol. Surv. Bull.* **2040**, 1-71 (1993).

24. Mosbrugger, V. & Utescher, T. The coexistence approach – a method for quantitative reconstructions of Tertiary terrestrial palaeoclimate data using plant fossils. *Paleogeogr. Palaeoclimatol. Palaeoecol.* **134**, 61–86 (1997).

25. Fauquette, S., *et al*. Latitudinal climatic gradients in the Western European and Mediterranean regions from the Mid-Miocene (c. 15 Ma) to the Mid-Pliocene (c. 3.5 Ma) as quantified from pollen data. [Williams, M., Haywood, A.M., Gregory, F.J., Schmidt, D.N. (eds.)] *Deep–Time Perspectives on Climate Change: Marrying the Signal from Computer Models and Biological Proxies*. The Micropalaeontological Society, Special Publications. The Geological Society, London, 481–502 (2007).

26 Bruch, A. A., T. Utescher, V. Mosbrugger, I. Gabrielyan, Ivanov, D.A. Late Miocene climate in the circum-Alpine realm--a quantitative analysis of terrestrial palaeofloras. *Palaeogeogr., Palaeoclimatol.,*

*Palaeoecol*. **238**, 270-280 (2006).

27 Grimm, G. W., & Denk, T. Reliability and resolution of the coexistence approach - A revalidation using modern-day data. *Rev. Palaeobot. Palyno*. **172**, 33-47 (2012).

28. Legates, D.R., & Willmott, C.J. Mean seasonal and spatial variability in global surface air temperature. *Theor. Appl. Climatol.* **41**, 11-21 (1990).

29 Haywood, A. M. & Valdes, P. J. Modelling middle Pliocene warmth: Contribution of atmosphere, oceans and cryosphere. *Earth Planet. Sci. Lett*. **218**, 363-377 (2004).

30. Jenness, J. & Wynne J.J. Cohen's Kappa and classification table metrics 2.0: an ArcView 3x extension for accuracy assessment of spatially explicit models. *U.S. Geol. Survey Open-File Report* **2005-1363** (2005).

31. Cohen, J. A coefficient of agreement for nominal scales. *Educ. Psychol. Meas.* **2**, 37–46 (1960).

32. Prentice, I.C., *et al.* A global biome model based on plant physiology and dominance, soil properties and climate. *J. Biogeogr.* **19**, 117-134 (1992).

33. Harrison, S.P., *et al.* Intercomparison of simulated global vegetation distributions in response to 6 kyr BP orbital forcing. *J. Climate* **11**, 2721-2742 (1998).

34. Monserud, R.A. & Leemans, R. Comparing global vegetation maps with the Kappa statistic. *Ecol. Model.* **62**, 275-293 (1992).

35. Harrison, S.P. & Prentice, I.C. Climate and $CO_2$ controls on global vegetation distribution at the last glacial maximum: analysis based on palaeovegetation data, biome modelling and palaeoclimate simulations. *Glob. Change Biol.* **9**, 983-1004 (2003).

36. Heinemann, M., et. al.: Warm Paleocene/Eocene climate as simulated in ECHAM5/MPI-OM, *Clim. Past* **5**, 785-802 (2009).

37. Lunt, D.J., et. al.: A model-data comparison for a multi-model ensemble of early Eocene atmosphere-ocean simulations: EoMIP. *Clim. Past Discuss*. **8**, 1229-1273 (2012).

38. Randall, D.A., et. al.: Climate Models and Their Evaluation. In: Climate Change 2007: The Physical Science Basis, Contribution of Working Group I to the Fourth Assessment Report of the Intergovernmental Panel on Climate Change [Solomon, S., Qin, D., Manning, M., Chen, Z., Marquis, M., Averyt, K.B., Tignor, M. and Miller, H.L. (eds.)]. Cambridge University Press, Cambridge, United Kingdom and New York, NY, USA (2007).

39. Haywood, A.M. et al. Large-scale features of Pliocene climate: results from the Pliocene Model Intercomparison Project. *Clim. Past*. **9**, 191-209 (2013).

40. Neale, R.B., et al. The mean climate of the Community Atmosphere Model (CAM4) in forced SST and fully coupled experiments. *J. Climate*, In Press, (2013)

41. Smith, R. D., *et al*. Parallel Ocean Program (POP) reference manual, Ocean component of the Community Climate System Model (CCSM). *Tech. Rep.* **LAUR-10-01853**, Los Alamos National Laboratory, Los Alamos, NM. (Available online at http://www.ccsm.ucar.edu/models/ccsm3.0/pop) (2010).

42. Danabasoglu, G., *et al.*: The CCSM4 Ocean Component. *J. Climate* **25**, 1361–1389 (2012).

43. Holland, M. M., et al. Improved sea ice shortwave radiation physics in CCSM4: The impact of melt ponds and black carbon. *J. Climate* **25**, 1413-1430, doi:10.1175/JCLI-D-11-00078.1 (2012).

44. Hunke, E.C. & Lipscomb, W.H. CICE: The Los Alamos Sea Ice Model. Documentation and Software User's Manual. Version 4.0. T-3 Fluid Dynamics Group, Los Alamos National Laboratory. *Tech. Rep.* **LA-CC-06-012** (2008).

45. Gent, P.R., et al. The Community Climate System Model version 4, *J. Climate*, 24, 4973-4991, 2012.

46. Oleson, K.W., *et al.* Improvements to the Community Land Model and their impact on the hydrological cycle. *J. Geophys. Res.*, **113**, G01021 (2008).

47. Stockli, R., *et al.* Use of FLUXNET in the Community Land Model development. *J. Geophys. Res.* **113**, G01025 (2008).

48. Rosenbloom, N.A., Otto-Bliesner B.L., Brady E.C. & Lawrence, P.J. Simulating the mid-Pliocene climate with the CCSM4 model. *Geosci. Model Dev. Disc*. **5**, 4269-4303 (2012).

49. K-1 Model Developers. *K-1 Coupled Model (MIROC) Description: K-1 Technical Report 1* (eds Hasumi, H. & Emori, S.). (Center for Climate System Research, University of Tokyo, 2004).

50. Oki, T. & Sud, Y. C. Design of Total Runoff Integrating Pathways (TRIP)—A Global River Channel Network. *Earth Interact.* **2**, 1–37 (1998).

51. Chan, W.-L., Abe-Ouchi, A. & Ohgaito, R. Simulating the mid-Pliocene climate with the MIROC general circulation model: experimental design and initial results. *Geosci. Model Dev.* **4**, 1035–1049 (2011).

52. Pope, V.D., Gallani, M.L., Rowntree, P.R. & Stratton, R.A. The impact of new physical parametrizations in the Hadley Centre Climate model: HadAM3. *Clim. Dynam.* **16**, 123-146 (2000).

53. Gordon, C. *et al.* The simulation of SST, sea ice extents and ocean heat transports in a version of the Hadley Centre coupled model without flux adjustments. *Clim. Dynam.* **16**, 147-168 (2000).

54. Cattle, H. & Crossley, J. Modelling arctic climate change. *Phil. Trans. R. Soc. A* **352**, 201-213 (1995).

55. Cox, P. M. *et al.* The impact of new land surface physics on the GCM simulation of climate and climate sensitivity. *Clim. Dynam.* **15**, 183-203 (1999).

56. Bragg, F.J., Lunt, D.J., & Haywood, A.M. Mid-Pliocene climate modelled using the UK Hadley Centre Model: PlioMIP Experiments 1 and 2. *Geosci. Model Dev. Discuss.* **5**, 837-871 (2012).

57. Schmidt, G.A. et al.: Configuration and assessment of the GISS ModelE2 contributions to the CMIP5 archive, in-preparation.

58. Hansen, J., *et al.,* Climate simulations for 1880-2003 with GISS modelE. *Clim. Dynam*. **29**, 661-696, doi:10.1007/s00382-007-0255-8 (2007).

59. Liu, J. *et al.* Sensitivity of sea ice to physical parameterizations in the GISS global climate model. *J. Geophys. Res.* **108**, 3053 (2003).

60. Kiang, N.Y., et al. A dynamic global terrestrial ecosystem model for coupling with GCMs, American Geophysical Union Fall Meeting. San Francisco, CA, December 10-15 (2006).

61. Chandler, M.A., *et al.,* Simulations of the Mid-Pliocene Warm Period using the NASA/GISS ModelE2-R Earth System Model. *Geosci. Model Dev. Discuss.* **5**, 2811-2842 (2012).

62. Roeckner, E., *et al.,* The atmospheric general circulation model ECHAM5, PART I: Model description, Report 349, Max-Planck-Institut fuer Meteorologie, Hamburg (2003).

63. Marsland, S.J., *et al.,* The Max-Planck-Institute global ocean/sea ice model with orthogonal curvilinear coordinates. *Ocean Modell*. **5**, 91–127 (2003).

64. Hibler, W.D.: A Dynamic Thermodynamic Sea Ice Model. *J. Phys. Oceanogr*. **9**, 815–846 (1979).

65. Jungclaus, J. H., *et al.,* Ocean Circulation and Tropical Variability in the Coupled Model ECHAM5/MPI-OM. *J. Climate* **19**, 3952–3972 (2006).

66. Raddatz, T.J., *et al.,* Will the tropical land biosphere dominate the climate-carbon cycle feedback during the twentyfirst century? *Clim. Dynam*. **29**, 565–574 (2007).

67. Hagemann, S. and Duemenil, L.: Documentation for the Hydrological Discharge Model, DKRZ *Technical Report No. 17*, Deutsches Klimarechenzentrum, Hamburg (1998).

68. Hagemann, S. and Gates, L. D.: Improving a subgrid runoff parameterization scheme for climate models by the use of high resolution data derived from satellite observations. *Clim. Dynam*. **21**, 349–359 (2003).

69. Stepanek, C. and Lohmann, G.: Modelling mid-Pliocene climate with COSMOS. *Geosci. Model Dev*. **5**, 1221–1243 (2012).

70. Hourdin, F., *et al.,* The LMDZ4 general circulation model: climate performance and sensitivity to parametrized physics with emphasis on tropical convection. *Clim. Dynam.* **27**, 787–813 (2006).

71. Hourdin F., *et al.,* Climate and sensitivity of the IPSL-CM5A coupled model: impact of the LMDZ atmospheric grid configuration. *Clim. Dynam.* In Press (2013).

72. Dufresne *et al.,* Climate change projections using the IPSL-CM5 Earth System Model: from CMIP3 to CMIP5. *Clim. Dynam*., In Press (2013).

73. Madec, G., *et al.,* OPA version 8.1 Ocean general circulation model reference manual, 3. LODYC, Technical Report, 91 pp. available at: http: //www.nemo-ocean.eu/About-NEMO/Reference-manuals, (1997).

74. Fichefet, T. and Morales-Maqueda, M. A.: Sensitivity of a global sea ice model to the treatment of ice thermodynamics and dynamics. *J. Geophys. Res*. **102**, 12609–12646 (1997).

75. Fichefet, T. and Morales-Maqueda, M. A.: Modelling the influence of snow accumulation and snow-ice formation on the seasonal cycle of the Antarctic sea-ice cover. *Clim. Dynam*. **15** 251–268 (1999).

76. Marti O., *et al.,* Key features of the IPSL ocean atmosphere model and its sensitivity to atmospheric resolution. *Clim. Dynam*. **34**, 1–26 (2010).

77. Krinner, G., *et al.,* A dynamic global vegetation model for studies of the coupled atmosphere-biosphere system. *Global Biogeochem. Cycles* **19**, GB1015, doi:10.1029/2003GB002199, (2005).

78. Contoux, C., *et al.,* Modelling the mid-Pliocene Warm Period climate with the IPSL coupled model and its atmospheric component LMDZ5A. *Geosci. Model Dev*. **5** (2012).

79. Yukimoto, S., *et al.,* Present-day and climate sensitivity in the meteorological research institute coupled GCM version 2.3 (MRI-CGCM2.3). *J. Meteorol. Soc. Japan* **84**, 333–363 (2006).

80. Mellor, G. L. and Kantha, L.: An ice-ocean coupled model. J. Geophys. Res. **94**, 10937–10954 (1989).

81. Sellers, P.J., *et al.,* A simple biosphere model (SiB) for use within general circulation models. *J. Atmos. Sci.* **43**, 505–531 (1986).

82. Sato, N., *et al.,* Effects of implementing the simple biosphere model in a general circulation model. *J. Atmos. Sci*. **46**, 2757–2782 (1989).

83. Kamae, Y. and Ueda, H.: Mid-Pliocene global climate simulation with MRI-CGCM2.3: set-up and initial results of PlioMIP Experiments 1 and 2. *Geosci. Model Dev.* **5**, 793-808 (2012).

84. Zhang, Z.S., *et al.,* Pre-industrial and mid-Pliocene simulations with NorESM-L. *Geosci. Model Dev.* **5***,* 523-533 (2012).

85. Dowsett, H.J. *et al*. Middle Pliocene paleoenvironmental reconstruction: PRISM2. *USGS Open File Report*, **99**-535(1999).

86. Rybczynski, N., Gosse, J.C., Harington, C.R., Wogelius, R.A., Hidy, A.J. & Buckley, M. Mid-Pliocene warm-period deposits in the High Arctic yield insight into camel evolution. *Nat. Commun.* **4**, 1550*, DOI: 10.1038/ncomms2516* (2013)

87. Ballantyne, A.P. *et al.* Significantly warmer Arctic surface temperatures during the Pliocene indicated by multiple independent proxies. *Geology* **38**, 603–606, (2010).

88. Fradkina, A.F. in *Abstracts of the Joint US/USSR Workshop on Pliocene Paleoclimates*. (eds. Thompson, R.S., Borisova, O.K. & Svetlitskaya, T.V.), pp. 22 (1991).

89. Nelson, R.E. & Carter, L.D. Pollen analysis of a late Pliocene & early Pleistocene section from the Gubik Formation of Arctic Alaska. *Quaternary Res.* **24**, 295-306 (1985).

90. Ager, T.A., Matthews, J.J.V. & Yeend, W. Pliocene terrace gravels of the ancestral Yukon River near Circle, Alaska: Palynology, paleobotany, paleoenvironmental reconstruction and regional correlation. *Quatern. Int.* **22-23**, 185-206 (1994).

91. Popova S., Utescher, T., Gromyko, D., Bruch, A.A. & Mosbrugger, V. Palaeoclimate Evolution in Siberia and the Russian Far East from the Oligocene to Pliocene – Evidence from Fruit and Seed Floras. *Turkish J. Earth Sci.* **21**, 315–334 (2012).

92. Volkova, V.S. in *Abstracts of the Joint US/USSR Workshop on Pliocene Paleoclimates*. (eds. Thompson, R.S., Borisova, O.K. & Svetlitskaya, T.V.), pp. 44-45 (1991).

93. Head, M.J. Pollen and dinoflagellates from the Red Crag at Walton-on-the-Naze, Essex; evidence for a mild climatic phase during the early late Pliocene of eastern England. *Geol. Mag.* **135**, 803-817 (1998).

94. Mai, D.H. & Walther, H., 1988. Die pliozänen Floren von Thüringen, Deutsche Demokratische Republik. *Quartärpaläontology* **7**, 55–297.

95. Willis, K.J., Kleczkowski, A. & Crowhurst, S.J. 124,000-year periodicity in terrestrial vegetation change during the late Pliocene epoch. *Nature* **397**, 685-688 (1999).

96. Wolfe, J.A. in *Pliocene Climates: Scenario for Global Warming*. (eds. Gosnell, L.B. & Poore, R.Z.), 39-42 (1990).

97. Fauquette, S., & Bertini, A. Quantification of the northern Italy Pliocene climate from pollen data: evidence for a very peculiar climate pattern. *Historical Biology* **32**, 361-369 (2003).

98. Fauquette, S., *et al.* Climate and biomes in the West Mediterranean area during the Pliocene. *Palaeogeogr. Palaeoclimatol. Palaeoecol.* **152**, 15-36 (1999).

99. Suc, J.P., & Cravatte, J. Etude palynologique du Pliocene de Catalogne (Nord-ouest de l'Espagne). *Paléobiologie continentale* **13**, 1-31 (1982).

100. Mamedov, A.V. in *Abstracts of the Joint US/USSR Workshop on Pliocene Paleoclimates*. (eds. Thompson, R.S., Borisova, O.K. & Svetlitskaya, T.V.), pp. 28 - 31 (1991).

101. Axelrod, D.I. The Sonoma Flora (California). *Publ. Carnegie Inst. Wash.* **553**, 167-206 (1944).

102. Thompson, R.S. Pliocene environments and climates in the western United States. *Quaternary Sci. Rev.* **10**, 115-132 (1991).

103. Iwauchi, A. Late Cenozoic vegetational and climatic changes in Kyushu, Japan. *Palaeogeogr. Palaeoclimatol. Palaeoecol.* **108**, 229-280 (1994).

104. Graham, A. & Dilcher, D.L. Studies in Neotropical paleobotany. XII. A palynoflora from the Pliocene Rio Banano Formation of Costa Rica and the Neogene vegetation of Mesoamerica. *Am. J. Bot.*, **85**, 1426-1438 (1998).

105. Martin, H.A. & McMinn, A. Palynology of Sites 815 and 823: the Neogene vegetation history of coastal north-eastern Australia. *P. Ocean Drill. Program, Sci Results* **133**, 115-123 (1993).

106. Macphail, M.K. Late Neogene climate in Australia. *Aust. J. Biol.* **45**, 425-460 (1997).

107. Kershaw, A.P. & Sluiter, I.R. Late Cenozoic Pollen Spectra from the Atherton Tableland, North-eastern Australia. *Aust. J. Bot.* **30**, 279-295 (1982).

108. Kershaw, P., Martin, H.A., & McEwen Mason, J.R.C. in *History of Australian Vegetation: Cretaceous to Recent*. (ed. Hill, R.S.), pp. 299 - 327. (Cambridge Univ. Press, Cambridge, 1994).

109. Dodson, J.R. & Macphail, M.K. Palynological evidence for aridity events and vegetation change during the Middle Pliocene, a warm period in Southwestern Australia. *Global Planet. Change* **41**, 285-307 (2004).

110. Macphail, M.K., Colhoun, E.A., & Fitzsimons, S.J. Key Periods in the Evolution of the Cenozoic Vegetation and Flora in Western Tasmania: the Late Pliocene. *Aust. J. Bot.* **43**, 505-526 (1995).

111. Sohl, L.E., *et al.* PRISM3/GISS topographic reconstruction. *U. S. Geol. Surv. Data Series* **419**, 6 pp., 2009.

112. Utescher, T. Mosbrugger, V. Palaeoflora Database. Available at http://www.palaeoflora.de (2010).

113. Demske, D., Mohr, B. & Oberhansli, H. Late Pliocene vegetation and climate of the Lake Baikal region, southern East Siberia, reconstructed from palynological data. *Palaeogeogr. Palaeoclimatol. Palaeoecol.* **184**, 107-129 (2002).

114. Utescher, T., Mosbrugger, V., & Ashraf, A.R. Terrestrial Climate Evolution in Northwest Germany over the Last 25 Million Years. *PALAIOS* **15**, 430-449 (2000).

115. Willard, D.A. Palynological record from the North Atlantic region at 3 Ma: vegetational distribution during a period of global warmth. *Rev. Palaeobot. Palyno.* **83**, 275-297 (1994).

116. Suc, J.P., *et al.* Zanclean (~Brunssumian) to early Piacenzian (~ early-middle Reuverian) climate from 4 to 54 north latitude (West Africa, West Europe and West Mediterranean areas). *Meded. Rijks Geol. Dienst.* **52**, 43-56 (1995).

117. Bonnefille, R., Potts, R., Chalie, F., Jolly, D. & Peyron, O. High-resolution vegetation and climate change associated with Pliocene Australopithecus afarensis. *P. Nat. Acad. Sci.* **101**, 12125-12129 (2004).

## 10. Supplementary Tables

**Table S1:** Details of models used for the terrestrial data/model comparison, details of boundary conditions as well as the climate sensitivity values (°C) for each model[39].

| Model ID, Vintage | Sponsor(s), Country | Atmosphere Top Resolution References | Ocean Resolution Z Coord., Top BC References | Sea Ice Dynamics, Leads, References | Coupling Flux adjust-ments, references | Land Soils, Plants, Routing, References | PlioMIP Experi-ment 2 [7] Preferred/ Alternate | Climate Sensi-tivity (°C) |
|---|---|---|---|---|---|---|---|---|
| CCSM4, 2010 | National Center for Atmospheric Research, USA | Top = 2.2 hPa 0.9x1.25°, L26 (40) | 1° x 1°, L60 Depth, free surface (41, 42) | Rheology, melt ponds (43, 44) | No adjustments (45) | Layers, canopy, routing (46, 47) | Alternate (48) | 3.2 |
| MIROC4m, 2004 | Center for Climate System Research (Uni. Tokyo, National Inst. for Env. Studies, Frontier Research Center for Global Change, JAMSTEC), Japan | Top = 30 km T42 (~ 2.8° x 2.8°) L20 (49) | 0.5° -1.4° x 1.4°, L43 Sigma/depth free surface (49) | Rheology, leads (49) | No adjustments (49) | Layers, canopy , routing (49, 50) | Preferred (51) | 4.05 |
| HadCM3, 1997 | Hadley Centre for Climate Prediction and Research/Met Office UK | Top = 5 hPa 2.5° x 3.75°, L19 (52) | 1.25° x 1.25°, L20 Depth, rigid lid (53) | Free drift, leads (54) | No adjustments (53) | Layers, canopy , routing (55) | Alternate (56) | 3.1 |
| GISS-E2-R, 2010 | NASA/GISS, USA | Top = 0.1 hPa 2˚ x 2.5˚, L40 (57) | 1˚ x 1.25˚, L32 Mass/area, free surface (58) | Rheology, leads (57, 59) | (57) | Layers, canopy, routing (60) | Preferred (61) | 2.7 to 2.9 |
| COSMOS COSMOS-landveg r 2413, 2009 | Alfred Wegener Institute, Germany | Top = 10 hPa T31 (3.75˚x 3.75˚), L19 (62) | Bipolar orthogonal curvilinear GR30, L40 (formal 3.0˚x 1.8˚) Depth, free surface (63) | Rheology, leads (63), following (64) | No adjustments (65) | Layers, canopy, routing (66, 67, 68) | Preferred (69) | 4.1 |
| IPSLCM5A, 2010 | Laboratoire des Sciences du Climat et de l'Environnement (LSCE), France | Top = 70 km 3.75° x 1.9°, L39 (70, 71) | 0.5°-2° x 2°, L31 Free surface, Z-coordinates (72, 73) | Thermodyna mics, Rheology, Leads (74, 75) | No adjustment (72, 75) | Layers, canopy, routing, phenology (72, 76, 77) | Alternate (78) | 3.4 |
| MRI-CGCM 2.3, 2006 | Meteorological Research Institute and University of Tsukuba, Japan | Top = 0.4 hPa T42 (~2.8° x 2.8°) L30 (79) | 0.5°-2.0° x 2.5°, L23 Depth, rigid lid (79) | Free drift, leads (80) | Heat, fresh water and momentum (12°S-12°N) (79) | Layers, canopy, routing (81, 82) | Alternate (83) | 3.2 |
| NorESM-L (CAM4), 2011 | Bjerknes Centre for Climate Research, Bergen, Norway | Top = 3.5 hPa T31 (~3.75° × 3.75°), L26 (CAM4) | G37 (~3° x 3° ), L30 isopycnal layers | Same as CCSM4 | Same as CCSM4 | Same as CCSM4 | Alternate (84) | 3.1 |

**Table S2**: Details of the additional orbital sensitivity experiments performed with HadCM3 and MIROC4m.

| Experiment | Description | PRISM2 (Boundary Conditions[50]) | PRISM3 (Boundary Conditions[7]) | Orbit (kyr) | $CO_2$ (ppmv) | Eccentricity | Precession | Obliquity (°) |
|---|---|---|---|---|---|---|---|---|
| $Plio^{PRISM}$ | Pliocene control simulation using PRISM boundary conditions[7]. | HadCM3 ($CO_2$ set at 400) | HadCM3 & MIROC4m | Modern | 405 | Modern | Modern | Modern |
| $Plio^{NHMax}_{400}$ | Pliocene simulation with maximum Pliocene incoming insolation at 65°N in July. | HadCM3 | HadCM3 & MIROC4m | 3037 | 400 | 0.051086 | -0.04239 | 23.642 |
| $Plio^{NHMax}_{450}$ | Pliocene simulation with maximum Pliocene incoming insolation at 65°N in July and high $CO_2$ levels. | HadCM3 | HadCM3 & MIROC4m | 3037 | 450 | 0.051086 | -0.04239 | 23.642 |
| $Plio^{SHMax}_{400}$ | Pliocene simulation with maximum Pliocene incoming insolation at 65°S in January. | HadCM3 | HadCM3 & MIROC4m | 3049 | 400 | 0.054523 | 0.05204 | 23.143 |
| $Plio^{SHMax}_{450}$ | Pliocene simulation with maximum Pliocene incoming insolation at 65°S in January and high $CO_2$ levels. | HadCM3 | HadCM3 & MIROC4m | 3049 | 450 | 0.054523 | 0.05204 | 23.143 |

**Table S3a**: Late Pliocene mean annual temperature estimates (SATs) from vegetation reconstructions. Temperature estimates for sites with modern altitude > 1000 m a.s.l. are not included.

| location | continent | latitude | longitude | altitude[a)] | age (Ma) | method[b)] | SAT | bioclim. range | temporal variability | confi-dence[c)] | reference |
|---|---|---|---|---|---|---|---|---|---|---|---|
| Beaver Pond/Ellesmere Isl. | North America | 78.40 | -82.00 | 350 | 3.8-3.4 | Multi-Proxies | -1.4 | ± 4.0 | n/a | 1 | 86, 87 |
| Lena River | Asia | 72.20 | 125.97 | 5 | 3.2-2.6 | QualEst | 1.5 | ± 1.0 | n/a | 4 | 88 |
| Ocean Point | North America | 70.00 | -153.00 | 308 | 2.7-2.6 | QualEst | 1.5 | n/a | n/a | 3 | 89 |
| Circle, Alaska | North America | 65.50 | -144.08 | 325 | 3.6-3 | QualEst | 3.0 | n/a | n/a | 3 | 90 |
| Blizkiy | Asia | 64.00 | 162.00 | 400 | 3.6-1.8 | CA | 5.3 | ± 5.8 | n/a | 3 | 91 |
| Nenana Valley, Alaska | North America | 64.53 | -149.08 | 295 | 3.6-2.8 | QualEst | 3.0 | n/a | n/a | 3 | 90 |
| Lost Chicken Mine | North America | 64.06 | -141.95 | 325 | 3.3-2.5 | QualEst | 2.5 | n/a | n/a | 3 | 90 |
| Delyankir | Asia | 63.00 | 133.00 | 600[a)] | 3.3-1.8 | CA | 7.4 | ± 0.5 | n/a | 3 | 91 |
| Magadan District | Asia | 59.98 | 150.65 | 97 | 3.2-2.6 | QualEst | 2.0 | n/a | n/a | 4 | 88 |
| West Siberia | Asia | 56.03 | 70.32 | 25 | 3.2-2.6 | QualEst | 13.5 | ± 1.5 | n/a | 4 | 92 |
| Merkutlinskiy | Asia | 56.00 | 72.00 | 50 | 3.3-1.8 | CA | 11.8 | ± 4.5 | n/a | 3 | 91 |
| Kabinet / 42km | Asia | 55.00 | 80.00 | 50 | 3.3-1.8 | CA | 8.9 | ± 2.3 | n/a | 3 | 91 |
| Mirny | Asia | 55.00 | 82.00 | 50 | 3.3-1.8 | CA | 11.2 | ± 1.3 | n/a | 3 | 91 |
| Maly-shik / Logovskoy | Asia | 54.00 | 81.00 | 50 | 3.3-1.8 | CA | 8.5 | ± 4.1 | n/a | 3 | 91 |
| Walton-on-the-Naze** | Europe | 51.84 | 1.27 | 25 | 3-2.6 | CA* | 12.8 | ± 1.3 | n/a | 2 | 93 |
| Willershausen | Europe | 51.77 | 10.10 | 212 | 3.2-2.6 | CLAMP, CA | 13.9 | ± 2.7 | n/a | 2 | 18 |
| Berga/Thuringia | Europe | 51.53 | 11.02 | 212 | 2.65-2.6 | CA | 13.5 | ± 0.5 | n/a | 3 | 18, 94 |
| Pula Maar | Europe | 47.05 | 17.38 | 200 | 3-2.98 | CA* | 12.8 | ± 1.2 | n/a | 1 | 95 |
| Oak Grove Forest | North America | 45.80 | -121.60 | 212 | 3.05-2.95 | CLAMP | 11.9 | ± 1.0 | n/a | 3 | 96,102 |
| Stirone | Europe | 44.60 | 10.15 | 779 | 2.8-2.6 | CAM | 15.0 | ± 2.0 | ± 3.0 | 1 | 97 |
| Pavlovskaya Depression | Asia | 44.09 | 132.09 | 200 | 3.2-2.6 | CA | 5.9 | ± 1.5 | n/a | 3 | 16 |
| Garraf, Catalonia | Europe | 41.17 | 2.02 | 62 | 3.6-3.2 | QualEst | 19.0 | n/a | n/a | 2 | 98,99 |
| Kura Depression | Europe | 40.53 | 49.69 | 226 | 3.2-2.6 | QualEst | 21.0 | n/a | n/a | 4 | 100 |
| California/Sonoma-Napa | North America | 38.30 | -122.45 | 313 | 3.45-3.35 | CLAMP | 17.6 | ± 2.0 | n/a | 3 | 101, 102 |
| Central Kyushu* | Asia | 33.10 | 131.50 | 149 | 2.9-2.8 | QuantEst | 18.0 | n/a | ± 1.0 | 2 | 103 |
| Rio Banano, Zent | North America | 10.03 | -83.28 | 12 | 3.6-2.6 | QualEst | 27.0 | n/a | n/a | 3 | 104 |
| ODP 823, Leg 133 (b)** | Australia | -16.69 | 145.21 | 190 | 3.2-2.6 | QualEst | 21.5 | ± 1.5 | n/a | 4 | 105, 106 |
| West Butcher Creek | Australia | -17.35 | 145.70 | 190 | 3.6-2.6 | QualEst | 21.2 | n/a | n/a | 3 | 107 |
| Lake George | Australia | -35.15 | 149.42 | 720 | 2.8-2.6 | QualEst | 14.0 | ± 2.0 | n/a | 3 | 106, 108 |
| Yallalie, Perth | Australia | -30.43 | 115.76 | 77 | 3.2-2.95 | QualEst | 21.0 | ± 5.0 | n/a | 2 | 109 |
| Linda Valley, Tasmania | Australia | -42.83 | 145.67 | 300[a)] | 3.6-2.5 | QualEst | 14.0 | ± 2.0 | n/a | 3 | 110 |

* corrected SAT at sea level after Iwauchi [103]

** land surface SAT of potential nearest terrestrial source area

n/a - no range or climate variability not identified

**Altitude[a)]**: Palaeoaltitude in masl., after Sohl *et al*.[111]

(modern altitude has been used for Chara Basin and Linda Valley)

**Key to confidence assessment[c)]**: 1 – very high, 2 – high, 3 - medium, 4 - low

**Key to "Methods[b)]"**

| | |
|---|---|
| QualEst | Qualitative estimates using modern analogues |
| CLAMP | Climate Leaf Analysis Multivariate Programe |
| CAM | Climate Amplitude Method |
| BA | Best Analogue/Plant Functional Type Method |
| QuantEst | Quantitative estimates using pollen indices |
| CA | Coexistence Approach |
| CA* | estimated from Palaeoflora Database [112] |

**Table S3b**: Late Pliocene mean annual temperature estimates (SATs) from vegetation reconstructions for sites providing information on temporal variability during the PRISM time slab (~3.3-3.0 Ma). Temperature estimates for marine sites more than 250 km away from mainland are not included.

| | | | | | | | | | | | | | Bioclim.Range + Temp. Variab.* | | |
|---|---|---|---|---|---|---|---|---|---|---|---|---|---|---|---|
| location | continent | latitude | longitude | altitude [a)] | age (Ma) | method [b)] | SAT | bioclim range | temporal variability | No of samples | confidence [c)] | reference | Method 1 | Method 2 (95%) | Method 2 (90%) |
| Chara Basin, Siberia | Asia | 56.97 | 118.31 | 700[a)] | 3.3-3.0 | QualEst | 12.8 | n/a | ± 1.8 | 17 | 2 | 17 | n/a | n/a | n/a |
| Lake Baikal | Asia | 55.69 | 108.37 | 450 | 3.3-3.0 | CA* | 7.0 | ± 2.5 | ± 3.0 | 12 | 1 | 113 | 3.91 | 4.28 | 3.77 |
| James Bay Lowland | North America | 52.83 | -83.88 | 50 | 3.3-3.0 | QualEst | 6.0 | ± 2.0 | ± 4.0 | >40 | 1 | 14 | 4.47 | 4.74 | 4.21 |
| Lower Rhine Basin | Europe | 51.03 | 6.53 | 135 | 3.6-2.6 | CLAMP, CA | 14.1 | ± 0.2 | ± 0.3 | 3 | 1 | 114 | 0.36 | 0.39 | 0.35 |
| Sessenheim-Auenheim | Europe | 48.82 | 8.01 | 297 | 3.6-2.6 | CA | 14.6 | ± 0.7 | ± 0.5 | 2 | 2 | 20 | 0.86 | 0.94 | 0.83 |
| Alpes-Maritimes | Europe | 43.82 | 7.19 | 193 | 3.3-3.2 | CAM | 17.5 | ± 2.0 | ± 0.5 | 18 | 2 | 99 | 2.06 | 2.05 | 1.87 |
| Tarragona | Europe | 40.83 | 1.13 | 401 | 3.3-3.0 | CAM | 20.0 | ± 2.5 | ± 2.5 | 3 | 2 | 99, 101 | 3.54 | 3.88 | 3.42 |
| Rio Maior | Europe | 39.35 | -8.93 | 42 | 3.6-3.0 | CAM | 16.0 | ± 2.0 | ± 2.0 | 17 | 1 | 99 | 2.83 | 3.11 | 2.74 |
| Yorktown, Virginia | North America | 36.59 | -76.38 | 57 | 3.5-2.9 | QualEst | 17.5 | n/a | ± 0.3 | 20 | 2 | 115 | n/a | n/a | n/a |
| Andalucia G1 | Europe | 36.38 | -4.75 | 305 | 3.6-2.6 | CAM | 21.0 | ± 2.0 | ± 3.5 | 12 | 1 | 99 | 4.03 | 4.32 | 3.83 |
| Habibas | Africa | 35.73 | -1.12 | 325 | 3.6-3.2 | CAM | 21.0 | ± 1.0 | ± 3.0 | >15 | 2 | 99, 116 | 3.16 | 3.23 | 2.90 |
| Nador | Africa | 35.18 | -2.93 | 206 | 3.6-2.6 | CAM | 21.5 | ± 1.0 | ± 3.0 | 7 | 1 | 99 | 3.16 | 3.23 | 2.90 |
| Pinecrest, Florida | North America | 27.36 | -82.44 | 10 | 3.5-2.6 | QualEst | 23.1 | n/a | ± 0.0 | 16 | 2 | 115 | n/a | n/a | n/a |
| Hadar | Africa | 11.29 | 40.63 | 849 | 3.4-2.9 | BA | 20.5 | ± 1.0 | ± 3.5 | 26 | 1 | 117 | 3.64 | 3.66 | 3.32 |

* - see Supplmentary Section 6 for description of Methods
**n/a** - no range or climate variability not identified

**Table S4:** Data-model comparison for BIOME4 HadCM3 and MIROC. Table shows difference between model and proxy-based mega-biome reconstructions using a warm (k-WB) and cold (k-CB) biased dataset. Kappa values [31] (κ) for global, polar, temperate tropical zones are ranked using a subjective assessment scale, whereby "0" means that the agreement is no better than would be expected by chance and "1" stands for a perfect match.

| Model | $R^2$ (SAT) | Global k-WB/k-CB | Polar k-WB/k-CB | Temperate k-WB/k-CB | Tropical k-WB/k-CB |
|---|---|---|---|---|---|
| **Pliocene HadCM3 PRISM2** | **0.85** | **0.31/0.25** | 0.01/0.00 | 0.29/0.21 | 0.03/0.01 |
| NH Max Orbit | 0.87 | **0.28/0.27** | 0.30/0.14 | 0.17/0.17 | 0.19/0.16 |
| SH Max Orbit | 0.85 | **0.30/0.26** | 0.00/0.00 | 0.26/0.21 | 0.11/0.09 |
| NH Max Orbit $CO_2$ 450 ppm | 0.87 | **0.31/0.26** | 0.42/0.21 | 0.21/0.16 | 0.15/0.12 |
| SH Max Orbit $CO_2$ 450 ppm | 0.85 | **0.33/0.30** | 0.03/0.00 | 0.26/0.23 | 0.16/0.14 |
| **Pliocene HadCM3 PRISM3** | **0.83** | **0.30/0.30** | 0.41/0.26 | 0.23/0.24 | 0.00/0.00 |
| NH Max Orbit | 0.84 | **0.25/0.25** | 0.24/0.14 | 0.17/0.18 | 0.14/0.12 |
| SH Max Orbit | 0.83 | **0.30/0.28** | 0.23/0.13 | 0.25/0.25 | 0.05/0.03 |
| NH Max Orbit $CO_2$ 450 ppm | 0.84 | **0.22/0.19** | 0.20/0.12 | 0.14/0.13 | 0.09/0.06 |
| SH Max Orbit $CO_2$ 450 ppm | 0.83 | **0.30/0.27** | 0.35/0.21 | 0.24/0.20 | 0.03/0.01 |
| **Pliocene MIROC PRISM3** | **0.83** | **0.30/0.27** | 0.36/0.22 | 0.21/0.18 | 0.06/0.05 |
| NH Max Orbit | 0.84 | **0.26/0.28** | 0.17/0.10 | 0.21/0.26 | 0.12/0.10 |
| SH Max Orbit | 0.83 | **0.29/0.27** | 0.15/0.00 | 0.21/0.20 | 0.06/0.04 |
| NH Max Orbit $CO_2$ 450 ppm | 0.84 | **0.25/0.26** | 0.12/0.06 | 0.22/0.25 | 0.11/0.08 |
| SH Max Orbit $CO_2$ 450 ppm | 0.83 | **0.29/0.27** | 0.30/0.18 | 0.20/0.18 | 0.06/0.04 |

**Supplementary Figure S1**

"Bioclimatic range" and "temporal variability" used for DMC. Fig S1 a) provides an example for a bioclimatic range produced by the Coexistence Approach, showing the mean annual temperature ranges tolerated by the nearest living relatives taxa A, B and C. The resulting temperature interval in which all taxa can coexist lies between 10.8 and 12.5°C (modified after [24]). b) shows the temporal variability caused by the variation of the reconstructed temperature over the geological period represented in the fossil record.

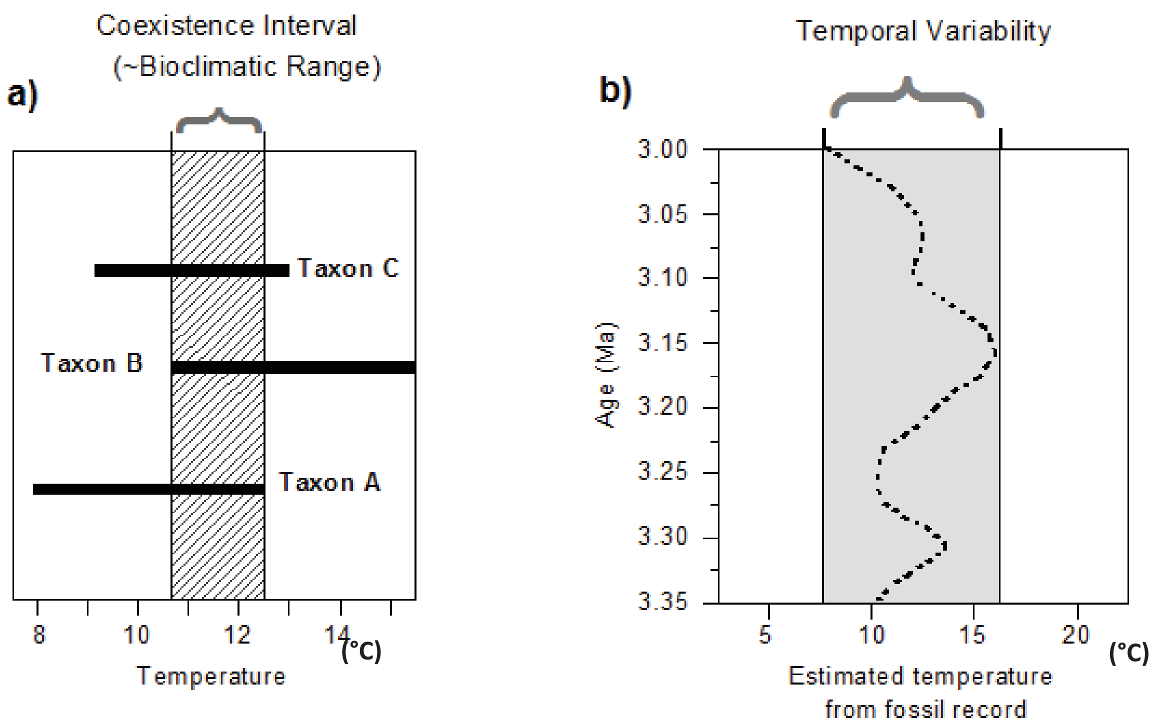

**Supplementary Figure S2**

Energy balance analysis for PlioMIP Experiment 2. Northern Hemisphere temperature change due to (a) clear sky albedo, (b) greenhouse gas emissivity, (c) cloud albedo and (d) cloud emissivity. PlioMIP Experiment 2 multi-model mean (MMM) is plotted in black, with the grey shading showing the range of values. Two warmest models (COSMOS and MIROC4m), as well as the two least warm (CCSM4 and MRI) are also shown.

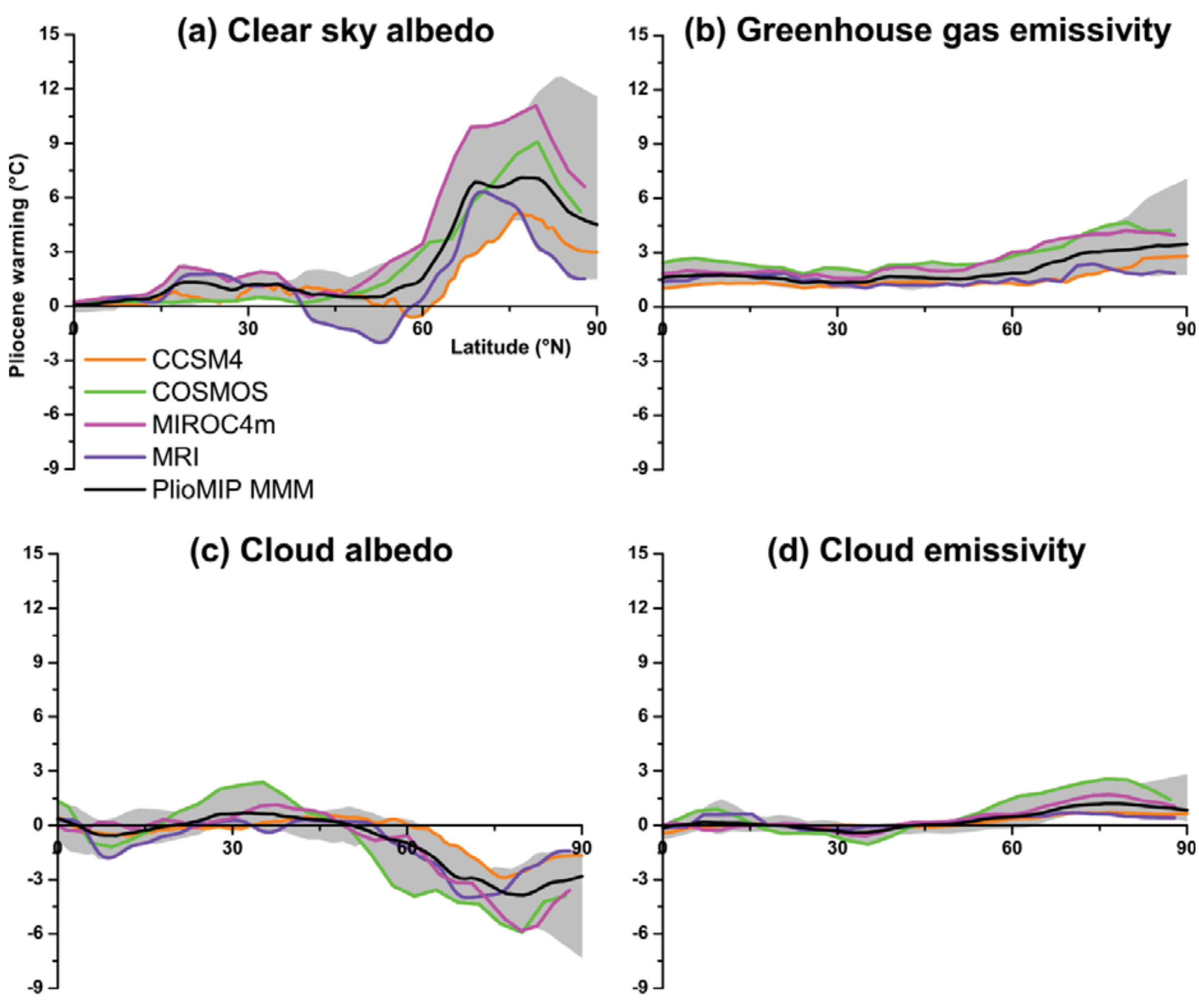

**Supplementary Figure S3**

Zonally averaged mean annual surface air temperatures (SAT) in °C derived from MIROC and HadCM3 simulations with varying boundary conditions from the PRISM3/2 dataset, changing orbital parameters and atmospheric $CO_2$-concentration. The Pliocene MMM is also displayed for reference.